

University of Calabria
School of Science and Technique "Bernardino Telesio"
Thesis of Doctoral Degree.

Organic Materials of Pharmacological Interest.

(XXV cycle)
CHIM06

Mechanism of Cell Wall Remodeling in
Mycobacterium tuberculosis.

Daniela Mavrici

December 2012

University of Calabria
School of Science and Technique "Bernardino Telesio"
Thesis of Doctoral Degree.

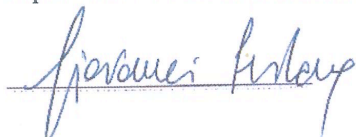
Organic Materials of Pharmacological Interest.

(XXV cycle)
CHIM06

Mechanism of Cell Wall Remodeling in
***Mycobacterium tuberculosis*.**

Daniela Mavrici

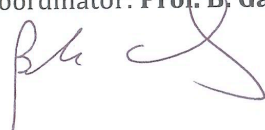
Supervisor: **Prof. G. Sindona**



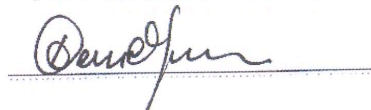
Co-supervisor: **Prof. T. Alber**



PhD Coordinator: **Prof. B. Gabriele**



PhD. Student: **D. Mavrici**



ABSTRACT

The spread of TB, as well as the rise of antibiotic resistance, create urgent needs for new therapeutics. Although potent antibiotics target the bacterial cell wall, surprisingly little is known about how this complex structure is built and degraded. The mechanisms that couple cell-wall remodeling to cell division and environmental cues also are poorly defined. These gaps in knowledge are particularly large for mycobacteria, which make a complex cell wall with many novel and unique structure. Mycobacteria also thrive in diverse niches, where cell-wall components vary to promote survival.

PG, a continuous sugar-peptide meshwork that forms an essential component of the cell wall, is a major focus of this project. Peptidoglycan key hydrolytic enzymes must be activated only at the right time and place to avoid the toxic destruction of the cell wall.

Most of the work presented here is focused on two classes of peptidoglycan hydrolases, NlpC/P60, a class of peptidases with 5 different genes encoded in *Mycobacterium tuberculosis*, and RpfB, resuscitation promoting factors, a class of lytic transglycosylases.

RipA (Rv1477), an NlpC/P60, is an essential peptidoglycan hydrolases in *Mtb* involved in cell elongation and division. Its activity must be highly regulated to allow cell survival. The crystal structure of RipA shows an enzyme in its inhibited form. We investigated in this work the possibility of activation by protein-protein interaction with RpfB and RpfE, as reported in literature. We solved the structure of RipB (Rv1478) at 1.64 Å of resolution. RipB is a protein homolog of RipA, encoded in

the same operon in *Mtb* genome. RipB shows the same inhibited form of RipA. Therefore the two proteins are very similar, but with the inhibitory section folded differently probably due to two different ways of activation.

We first proved and then extensively investigated the interaction between Rv2190c, another NlpC/P60 peptidase, and FtsX, a predicted ABC transporter.

FtsX is an essential protein, conserved in all bacteria but the real function of this protein is still unknown. In *E. coli* FtsX interacts with FtsE, a cytoplasmatic ATP binding protein, essential for cell division under low osmolarity condition. Depletion of FtsX and mutations in FtsE ATP binding cassette does not allow *E. coli* to divide with formation of long branched cells. The model proposed is that ATP binds FtsE inside the cell causing a cascade of conformational changes through the membrane directed towards periplasm, where the ultimate step is to switch enzymes from the inactive conformation to the active one. The very intriguing hypothesis is that the hydrolysis of ATP inside the cell controls the hydrolysis of peptidoglycan outside the cell.

We performed experiments *in vitro* between the two proteins to elucidate the kind of interaction and to understand the function of the interaction between Rv2190c and FtsX. We assemble the complex *in vitro* showing that only the N terminus of Rv2190c interacts with FtsX. Limited proteolysis experiments show conformational changes for Rv2190c in presence of FtsX. We were able also to crystallize the complex but it diffracted between 14 and 8 Å of resolution. Further experiments are necessary to solve the structure of the complex.

Finally, we solved the structure of RpfE, resuscitation promoting factor E at 2.76 Å of resolution. The protein is a small lytic transglycosylase very similar in folding with RpfB, another Rpf factor of *Mtb*.

Even though, the two enzymes are very similar in the catalytic domain folding, RpfE shows a catalytic cleft with a complete different charge state. While RpfB presents a very negative charged patches surface along all the catalytic cleft, RpfE instead

shows a positive charge catalytic cleft. This difference might denote difference in substrate binding.

Alltogether, these studies generate new insights into cell wall remodeling and specifically in peptidoglycan hydrolases mechanism in mycobacteria. By elucidating their crystal structures, we better understand the way these enzyme work and rise new hypothesis on how they are regulated *in vivo*.

*To my Mother,
for believing always in me and encouraging to pursue my dreams.*

ACKNOWLEDGEMENTS

I would like to thank first the University of Calabria and the Department of Chemistry. Professor Giovanni Sindona, who allowed me to pursue this wonderful research experience abroad.

I would like also to thank Professor Bartolo Gabriele and the School of Science and Technique “B. Telesio”. Professor Gabriele was very kind also to help me solving all the problems related with paperwork. I would like to thank University of California at Berkeley as well for hosting me.

I am grateful also to Dr. Lori Kohlstaedt who first gave me an opportunity in Berkeley, when I arrived from Italy six years ago. Lori introduced me to the work in a foreigner country and helped to get accustomed to a new life environment. She always encouraged me to pursue a doctoral degree.

I would like to thank all the people who helped to solve technical problems during my work. Abbey Hartland, Macrolab, Tony Iavarone, and Bertozzi Lab members who allowed me to use their instruments.

My graduate school experience would not be the same without all the wonderful people I met in the Alber Lab. Alejandra Cavazos, Ursula Schulze-Gahmen, Megan Flynn, John Huizar, Alex Scouras, Terry Lang, and Ho Jun Lee for their technical support and help; Daniil Prigozhin for help and scientific discussion about our project; Christina Baer who assisted me in the early months in the Alber Lab helping with the transition from mass spectrometry to molecular biology. Of course, this journey wouldn't be the same without the friends I met in the lab, Seemay Chou, Katherine Bao, Heather Upton, and Avi Samelson, all helped me and gave a touch of life that I was missing since I arrived in this country. Kat was also a wonderful lab manager who accommodated my requests.

A big thanks goes to my husband, Francesco. Without him all of this would have not been possible. He funded initially my graduated fellowship and encouraged me all the time, relentlessly. He was always patient and supportive, willing to help me at any moment. A special thanks goes also to my family, so far away from here but always present and supportive.

Lastly, I would like to express my sincere gratitude to Tom Alber, who allowed me to join his lab and to pursue this exciting experience in a multidisciplinary environment. I thank him for being an excellent mentor, always ready to provide advices and suggestions. His love for science always pervades me with enthusiasm. Thanks Tom!

TABLES OF CONTENTS

CHAPTER	Page
1. MYCOBACTERIAL CELL WALL.....	1
1.1. Introduction.....	2
1.2. Figures.....	7
1.3. References.....	9
2. MYCOBACTERIUM TUBERCULOSIS PEPTIDOGLYCAN HYDROLASES: ACTIVATION BY PROTEIN-PROTEIN INTERACTION	12
2.1 Introduction.....	13
2.2 Looking for protein complexes.....	16
2.3 Rv1478 and RpfD interaction.....	17
2.4 RpfD refolding strategy.....	18
2.5 RpfB and RipA interaction.....	19
2.6 Rv1478/RipB structure.....	20
2.7 Discussion.....	22
2.8 Materials and Methods.....	24
2.9 Figures.....	33
2.10 Tables.....	45
2.11 References.....	51
3 FTSX-RV2190C COMPLEX.....	53
3.1 Introduction.....	54
3.2 Results.....	57
3.3 Limited proteolysis of the complex Rv2190c and FtsX.....	58
3.4 Rv2190c crystallization.....	60
3.5 Rv2190c-FtsX crystallization.....	60
3.6 Discussion.....	63
3.7 Materials and Methods.....	65
3.8 Figures.....	67

3.9 Tables.....	74
3.10 References.....	75
4 RPF E CRYSTAL STRUCTURE REVEALS A POSITIVELY CHARGED	
CATALYTIC CLEFT.....	77
4.1 Introduction.....	78
4.2 RpfE and RipA interaction.....	80
4.3 RpfE structure.....	80
4.4 Comparison between RpfB and Rpf.....	81
4.5 Discussion.....	83
4.6 Material and Methods.....	85
4.7 Figures.....	87
4.8 Tables.....	92
4.9 References.....	93

Chapter 1

Mycobacterial cell wall.

1.1 Introduction.

Bacterial cell wall envelopes are complex structures that delimit cells and protect them from the environment. Classification of bacteria as Gram positive or Gram negative is based on the architecture of the cell wall^{1,2}. Gram-negative cell envelopes are formed by a thin layer of peptidoglycan and a thick outer membrane that is covalently linked to a core of saccharides. In these organisms, the outer membrane plays very important roles in protecting the cell from toxic molecules and providing an additional stabilizing layer around the organism³. Gram-positive bacteria, in contrast, have a thick layer of peptidoglycan to resist and survive in extreme environmental conditions. Gram-positive cell envelopes are decorated by other small entities, such as teichoic acids^{4,5}.

Corynebacterineae represent a special family of bacteria, from the point of view of the cell-envelope architecture. They usually present a very complex cell wall with characteristics of both Gram-positive and -negative bacteria^{6,7}. *Corynebacterineae* include very important pathogens such as *Mycobacterium tuberculosis* and *Mycobacterium leprae*. These organisms respectively cause tuberculosis (TB) and leprosy, which are among the most ancient diseases reported in history. Antibiotics that completely kill Mycobacteria do not exist.

Mycobacterium tuberculosis is one of the most successful bacteria to escape drug control and resist antibiotics^{8,9}. This bacterium kills more than two million people every year worldwide, and more than one third of the population carries a latent infection, making urgent the development of new drugs against TB¹⁰. The peculiarity that makes Mycobacteria so successful against drugs is the complexity of its cell envelope. Little is known about this complex structure, the way is built and degraded. The mechanism that couples cell-wall assembly and remodeling to cell division is mostly undefined^{11,12}.

Many classes of TB antibiotics target the Mycobacterial cell wall¹³. Like other *Corynebacterineae*, Mycobacteria synthesize cell envelopes with different

compositions and greater complexity compared to other bacteria¹⁴. Outside the cellular membrane, Mycobacterial cell walls are composed of four layers (Figure 1). The first layer is Peptidoglycan (PG). PG is composed of carbohydrate polymer strands cross-linked by short peptides^{8,9}. Even though PG is a very stable structure due to the covalent cross-linking, dynamic remodeling occurs during cell growth and division. The second layer, arabinogalactan (AG) contains arabinan and galactan polymers covalently attached to PG. Covalently linked to the AG, the third layer contains mycolic acids (MAs) consisting of long-chain hydroxy fatty acids^{15,16}. The last layer has been recently discovered and is called the capsule, composed of arabinomannan, α -glucan and oligomannosyl-capped glycolipids important for binding cells during infection⁹.

Among the numerous functions, the cell envelope provides structural rigidity that determines cell shape, allows the cell to resist osmotic pressure, protects the cell from external insults and promotes infection in the host by a sophisticated mechanism that is still unknown. Due to the high complexity of the cell-wall architecture, many enzymes are involved in cell wall biogenesis. Even though many efforts have been made to elucidate individual reactions that contribute to cell wall synthesis, degradation, and maintenance^{8,9}, many additional essential pathways need to be discovered to better understand and describe the whole envelope. Moreover, little is known about the assembly and remodeling of these different layers. How are the enzymes responsible for these processes coordinated? How are the different layers built in conjunction with cell growth and split during cell division?

Mycobacterium tuberculosis is a rod-shaped bacterium, but cell septation and division do not occur in the middle of the cell generating two equal daughter cells., *Mtb* grows asymmetrically at one tip, generating two different daughter cells. One inherits the growing pole from the mother, and the other one develops a pole able to separate. In the latter cell type, the growing pole alternates in each generation, and a significant portion of the cell envelope is recycled¹⁷.

Even though the cell envelope looks like a static and rigid mesh, it is actively remodeled and adjusted to be inherited by the new cell, making it a very dynamic structure¹⁸. The mechanisms of spatial and temporal regulation of envelope biogenesis is not understood. This work is focused on the first layer of *Mycobacterium tuberculosis* cell envelope and more precisely on peptidoglycan remodeling in *Mycobacterium tuberculosis*.

Peptidoglycan remodeling consists of two distinct processes: synthesis and degradation. During cell growth, newly synthesized PG is attached to the sacculus. To allow the sacculus to elongate and not just increase in thickness, cleavages of covalent bonds are required¹⁹. This role is performed by PG hydrolases, a class of enzyme involved in many different processes in PG biogenesis. PG hydrolases are involved in sculpting cell shape, recycling much of the PG in each generation, creating gaps for protein insertion and splitting PG during cell division²⁰. Since they degrade PG, the hydrolases are potentially toxic to the cell and they have to be highly regulated and coordinated with biosynthetic enzymes to avoid cell lysis²¹.

Different classes of PG hydrolases cleave bonds that link each of the building blocks of PG. The hydrolases are classified in three different categories, depending on the type of linkage that is cleaved (Figure 2). The amidases are responsible for cleaving sugar-peptide linkage; glycosidases and transglycosidases are responsible for cleaving sugar chains and finally peptidases degrade peptide bonds. PG peptidases are categorized as peptidases and carboxypeptidases^{5,22}.

We identified 22 *Mtb* homologs by searching the *Mtb* genome with the HMMER3 program using Hidden Markov Models^{23,24} of the catalytic domains of the three PG hydrolase classes. As in *E. coli*, many of the PG hydrolases show redundant functions. Based on high-resolution transposon mutagenesis²⁵, it is possible to identify only 4 of the 22 PG hydrolases as essential enzymes in *Mtb*. These four proteins (Rv3915, Rv1477, Rv3627c and Rv3593) are essential for growth.

PG hydrolases have been studied in a range of different bacteria, and in all the systems, these proteins show high redundancy. For this reason, it is difficult to study the role of single PG hydrolase. Moreover, no single hydrolase gene knockout prevents growth. In *E. coli*, for example, multiple PG hydrolase genes have to be deleted to get chains of unseparated cells^{26,27}. Recent studies in a wide range of bacteria are beginning to uncover their diverse roles in the cell²⁰.

Uncontrolled PG hydrolase activity would disrupt the sacculus and lyse the cell. The newly emerging models show that this class of enzymes has to be regulated and their function highly coordinated with PG synthases²⁸. The regulation is likely to be widespread among bacteria. So far, two main models have been reported. In the first one, involving activation by protein-protein interactions, each hydrolase is part of a multiprotein complex and the hydrolytic activity is controlled by its incorporation within this complex. The complex localizes only at the site of PG synthesis and prevents hydrolysis of peptidoglycan elsewhere^{21,29}. In the second model, PG hydrolases are held in check by inhibitor proteins. For example, bacteria utilize PG hydrolases to attack other bacteria in a fratricidal war. The hydrolases, to spare the periplasm of producer cells, are bound to an inhibitor protein that protects against direct hydrolase activity and directs activity to different bacteria³⁰. Similarly, inhibitory complexes may be disassembled specifically at sites of cell growth and division.

In *Mycobacterium tuberculosis*, an activating interaction between two PG hydrolases, RipA (Rv1477) and RpfB or RpfE (Rv1009, Rv2450c) has been reported. RipA also has been reported to interact with the trans-peptidase domain of PBP1, a PG synthase enzyme. RipA, which is inactive in isolation, interacts with PBP1 at the septum during cell elongation and PG synthesis, and once the daughter cells are completely formed, interacts with RpfB to split the two cells just formed^{31,32}.

Here, I report a body of work aimed at expanding our biochemical and structural

understanding of *Mycobacterium tuberculosis* PG hydrolases *in vitro*. My approach was to explore interactions between hydrolases and other proteins to test for protein-protein interactions that activate these enzymes. I largely explored the interaction *in vitro* between RipA and RpfB-E and between RipB and RpfD. I solved the crystal structures of RipB and RpfE. Both structures provide insights into the mechanisms of activation. RipB was autoinhibited and required dissociation of a peptide from the active site to enable substrate binding. RpfE, on the other hand, exhibits a very similar fold as RpfB, but a completely different enzymatic cleft, with intrinsic discrimination for substrate.

I discovered an interaction between FtsX and Rv2190c and I extensively investigated the mechanism of complex assembly. Between RipA and Rv2190c in *Mtb*, only Rv2190c binds to FtsX, showing the complexity and specificity of PG hydrolase regulation. The FtsX-Rv2190c complex opens up a new intriguing hypothesis regarding the regulation of PG degradation. Interestingly, FtsX is homologous to an *E. coli* integral membrane protein interacting in the cytoplasm with FtsE (an ATP binding protein) and the lack of ATP hydrolysis produces long branches of unseparated *E. coli*³³ cells. Deep and exhaustive investigation of this FtsEX -Rv2190c complex would offer the first evidence regarding the hydrolysis of ATP in the cytoplasm and the effects on the periplasmatic hydrolysis of PG.

1.2 Figures.

Figure 1. Mycobacterial cell wall.

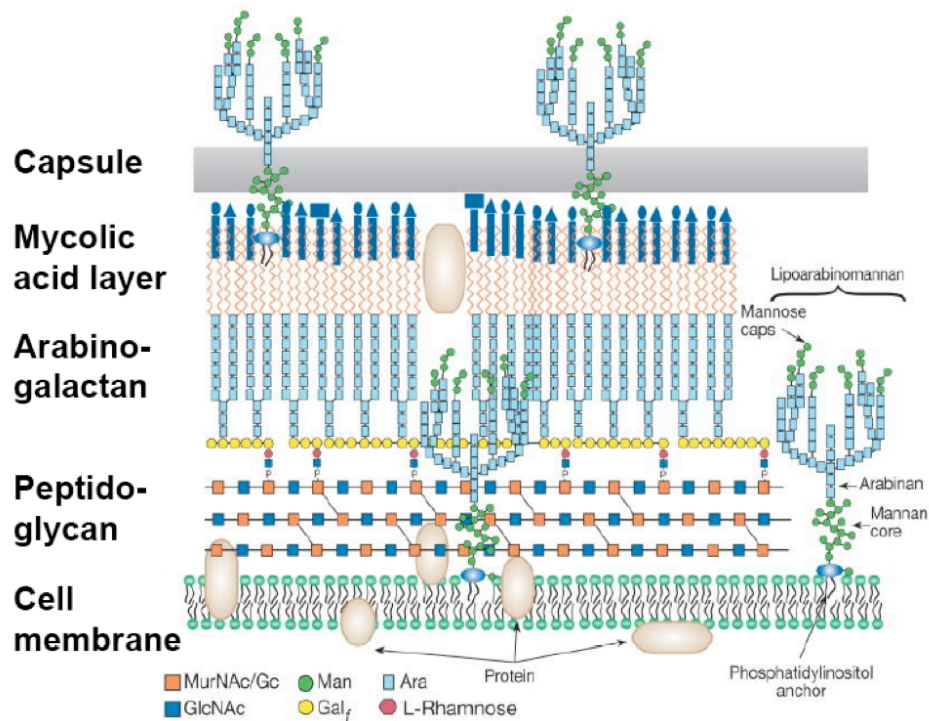


Figure 1. Mycobacterial cell wall. Mycobacteria cell wall consists of two segments. The lower segment extends beyond the membrane, with peptidoglycan (PG) forming a very complex network around the cell. As seen on the figure above, arabinogalactan (AG) is covalently attached to PG and mycolic acid in turn is covalently attached to AG. The upper segment is composed of free lipids, cell wall proteins, phosphatidylinositol mannosides (PIMs), lipomannans (LM) and lipoarabinomannan (LAM)¹⁴.

Figure 2. *Mycobacterium tuberculosis* Peptidoglycan.

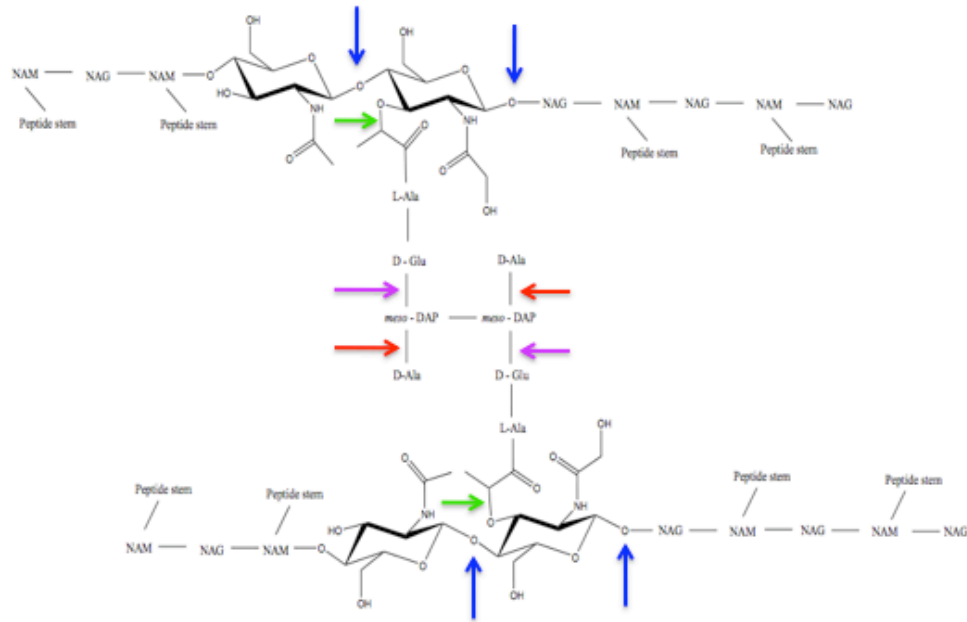


Figure 2. *Mycobacterium tuberculosis* Peptidoglycan. *Mycobacterium tuberculosis* peptidoglycan consists of long glycan strands composed by repeating N-acetylglucosamines (NAG) linked to N-acetylmuramic acids. These strands are cross-linked to the lactyl group of NAM from different glycan strands. Peptide chains normally consist of a L-alanyl-D-isoglutaminyl-meso-diaminopimelic acid (DAP) linked to a terminal D-alanine residue from L-alanyl-D-isoglutaminyl-meso-DAP-D-alanine. Typically, Gram-positive bacteria such as *Mycobacteria* incorporate lysine as a unique basic amino acid residue. Alternatively, *Mycobacteria* incorporate diaminopimelic (DAP) acid, which is typical of Gram-negative bacteria. *Mycobacterial* peptidoglycan show modifications that make it unique. More specifically, it has been reported that N-acetyl group on muramic acid is sometimes modified by a N-glycolyl group. Moreover, on average 25% of PG is 3-3 crosslinked (DAP-DAP) in *Mycobacteria*, with the rest being typically 3-4 (DAP-Ala) crosslinked. In other bacteria such as *E. coli*, only a small portion of peptidoglycan is crosslinked and the ratio of crosslinked PG over the uncrosslinked increase with the resistance to antibiotics.

1.3 References.

- ¹ Rothfield, "Biological membranes: An overview at the molecular level. In Structure and function of biological membranes," 3 – 9 *Academic Press Inc*, New York., (1971).
- ² Silhavy TJ, Kahne D, Walker S., "The bacterial cell envelope." *Cold Spring Harb Perspect Biol*. May;2(5), no. 2010 Apr 14. (2010).
- ³ Glauert AM, Thornley MJ., "The topography of the bacterial cell wall." *Annu Rev Microbiol* 23 (1969): 159 – 198.
- ⁴ Vollmer W, Blanot D, de Pedro MA., "Peptidoglycan structure and architecture." *FEMS Microbiol Rev*, no. 32 (2008.): 149 – 167.
- ⁵ Vollmer W., "Structural variation in the glycan strands of bacterial peptidoglycan." *FEMS Microbiol Rev*, no. 32 (2008): 287 – 306.
- ⁶ Fu LM, Fu-Liu CS., "Is *Mycobacterium tuberculosis* a closer relative to Gram-positive or Gram-negative bacterial pathogens?" *Tuberculosis* 82 (2002.): 85 – 90.
- ⁷ Ratledge C., Stanford J., "The biology of the mycobacteria-Physiology, identification and classification." *Academic Press, Inc.*, New York, NY. vol1 (1982).
- ⁸ Kaur, D., Guerin, M. E., Skovierova, H., Brennan, P. J., and Jackson, M., "Chapter 2: Biogenesis of the cell wall and other glycoconjugates of *Mycobacterium tuberculosis*." *Adv Appl Microbiol* 69 (2009): 23-78.
- ⁹ Sani, M., Houben, E. N., Geurtsen, J., Pierson, J., de Punder, K., van Zon, M., Wever, B., Piersma, S. R., Jimenez, C. R., Daffe, M., Appelmek, B. J., Bitter, W., van der Wel, N., and Peters, P. J. "Direct visualization by cryo-EM of the mycobacterial capsular layer: a labile structure containing ESX-1-secreted proteins." *PLoS Pathog* 6 (2010): e1000794.
- ¹⁰ Vilcheze, C., Baughn, A. D., Tufariello, J., Leung, L. W., Kuo, M., Basler, C. F., Alland, D., Sacchetti, J. C., Freundlich, J. S., and Jacobs, W. R., Jr., "Novel inhibitors of InhA efficiently kill *Mycobacterium tuberculosis* under aerobic and anaerobic conditions." *Antimicrob Agents Chemother* 55 (2011): 3889-3898.
- ¹¹ Lavollay, M., Arthur, M., Fourceaud, M., Dubost, L., Marie, A., Veziris, N., Blanot, D., Gutmann, L., and Mainardi, J. L., "The peptidoglycan of stationary-phase *Mycobacterium tuberculosis* predominantly contains cross-links generated by L,D-transpeptidation." *J Bacteriol* 190 (2008): 4360-4366.
- ¹² Magnet, S., Arbeloa, A., Mainardi, J. L., Hugonnet, J. E., Fourceaud, M., Dubost, L., Marie, A., Delfosse, V., Mayer, C., Rice, L. B., and Arthur, M., "Specificity of L,D-transpeptidases from gram-positive bacteria producing different peptidoglycan chemotypes." *J Biol Chem* 282 (2007): 13151-13159.
- ¹³ Schneider, T., and Sahl, H. G., "An oldie but a goodie - cell wall biosynthesis as antibiotic target pathway." *Int J Med Microbiol* 300 (2010): 161-169.
- ¹⁴ Hett EC, Rubin EJ., "Bacterial growth and cell division: a mycobacterial perspective." *Microbiol Mol Biol Rev*. Mar;72(1) (2008): 126-56.
- ¹⁵ Brennan, P. J., "Structure, function, and biogenesis of the cell wall of *Mycobacterium tuberculosis*." *Tuberculosis* 83 (2003): 91–97.
- ¹⁶ Brennan, P. J., and H. Nikaido., "The envelope of mycobacteria." *Annu Rev. Biochem.* 64 (1995): 29–63.

-
- ¹⁷ Aldridge BB, Fernandez-Suarez M, Heller D, Ambravaneswaran V, Irimia D, Toner M, Fortune SM., "Asymmetry and aging of mycobacterial cells lead to variable growth and antibiotic susceptibility." *Science* Jan 6;335(6064) (2012): 100-4.
- ¹⁸ Park, J. T., and Uehara, T., "How bacteria consume their own exoskeletons turnover and recycling of cell wall peptidoglycan" *Microbiol Mol Biol Rev* 72 (2008): 211-227.
- ¹⁹ Holtje, J. V., "Growth of the stress-bearing and shape-maintaining murein sacculus of *Escherichia coli*." *Microbiol Mol Biol Rev* 62 (1998): 181-203.
- ²⁰ Typas A, Banzhaf M, Gross CA, Vollmer W., "From the regulation of peptidoglycan synthesis to bacterial growth and morphology." *Nat Rev Microbiol.* Dec 28;10(2) (2011): 123-36.
- ²¹ Morlot, C., Uehara, T., Marquis, K. A., Bernhardt, T. G., and Rudner, D. Z., "A highly coordinated cell wall degradation machine governs spore morphogenesis in *Bacillus subtilis*." *Genes Dev* 24 (2010): 411-422.
- ²² van Heijenoort J. "Peptidoglycan hydrolases of *Escherichia coli*." *Microbiol Mol Biol Rev* 75(4) (2011): 636-63.
- ²³ Eddy, S. R., "A new generation of homology search tools based on probabilistic inference." *Genome Inform* 23 (2009): 205-211.
- ²⁴ Finn, R. D., Mistry, J., Tate, J., Coggill, P., Heger, A., Pollington, J. E., Gavin, O. L., Gunasekaran, P., Ceric, G., Forslund, K., Holm, L., Sonnhammer, E. L., Eddy, S. R., and Bateman, A., "The Pfam protein families database." *Nucleic Acids Res* 38 (2010): D211-222.
- ²⁵ Sasseti CM, Boyd DH, Rubin EJ., "Comprehensive identification of conditionally essential genes in mycobacteria." *Proc Natl Acad Sci U S A.* Oct 23;98(22) (2001): 12712-7.
- ²⁶ Priyadarshini R, Popham DL, Young KD., "Daughter cell separation by penicillin-binding proteins and peptidoglycan amidases in *Escherichia coli*." *J Bacteriol.* Aug;188(15) (2006): 5345-55.
- ²⁷ Heidrich C, Templin MF, Ursinus A, Merdanovic M, Berger J, Schwarz H, de Pedro MA, Höltje JV., "Involvement of N-acetylmuramyl-L-alanine amidases in cell separation and antibiotic-induced autolysis of *Escherichia coli*." *Mol Microbiol.* Jul;41(1) (2001): 167-78.
- ²⁸ Uehara T, Bernhardt TG. , "More than just lysins: peptidoglycan hydrolases tailor the cell wall." *Curr Opin Microbiol.* Dec;14(6) (2011): 698-703.
- ²⁹ Uehara T, Parzych KR, Dinh T, Bernhardt TG., "Daughter cell separation is controlled by cytokinetic ring-activated cell wall hydrolysis." *EMBO J.* Apr 21;29(8) (2010): 1412-22.
- ³⁰ Russell AB, Hood RD, Bui NK, LeRoux M, Vollmer W, Mougous JD., "Type VI secretion delivers bacteriolytic effectors to target cells." *Nature.* Jul 20;475(7356) (2011): 343-7.
- ³¹ Hett EC, Chao MC, Deng LL, Rubin EJ., "A mycobacterial enzyme essential for cell division synergizes with resuscitation-promoting factor." *PLoS Pathog.* Feb 29;4(2) (2008): e1000001.

³² Hett EC, Chao MC, Rubin EJ., "Interaction and modulation of two antagonistic cell wall enzymes of mycobacteria." *PLoS Pathog.* Jul 29;6(7) (2010): e1001020.

³³ Yang DC, Peters NT, Parzych KR, Uehara T, Markovski M, Bernhardt TG., "An ATP-binding cassette transporter-like complex governs cell-wall hydrolysis at the bacterial cytokinetic ring.," *Proc Natl Acad Sci U S A.* Nov 8;108(45) (2011): E1052-60.

Chapter 2

***Mycobacterium tuberculosis* peptidoglycan hydrolases:
Activation by protein-protein interaction.**

2.1 Introduction.

Peptidoglycan hydrolases is a class of enzymes involved in many processes of bacterial cells like growth, cell division, septation, cell-wall recycling and signaling^{1,2,3,4}. Although PG hydrolases were for long time associated with cell degradation, like lysozyme, new developments on this class of enzyme are raising the intriguing question of how PG hydrolytic activity is regulated to avoid cell disintegration⁵.

In the last few years, several cases of highly regulated PG hydrolases have been reported^{6,7,8}. In *Bacillum subtilis*, it has been postulated that the SpoIIP-SpoIID complex pulls the mother cell membrane around the forespore with the subsequent direction of PG machinery from the mother to the forespore⁹. Although the *in vivo* mechanism remains unclear, the *in vitro* activity has been well investigated⁷. SpoIIP was predicted to have amidase and endopeptidase activity and SpoIID transglycosylase activity. Briefly, SpoIID can bind PG, but no activity is detected until the stem peptide has been removed by SpoIIP. On the other hand, the activity of SpoIIP is achieved by the interaction with SpoIID. The interaction between the two proteins is indispensable for complex activation and regulation.

Complexes between two PG hydrolases have been reported also for *Mycobacterium tuberculosis*. Rubin and coworkers reported a case of interaction between RpfB – resuscitation promoting factor B - and an NlpC/P60 L-D endopeptidase called RipA^{8,10,11}. Based on yeast two-hybrid assay, RipA interacts with RpfB and RpfE, two resuscitation promoting factors, and PBP1, an the essential high-molecular-weight PG synthase. The region of RipA involved in all these interactions is the C-terminus of the catalytic domain. Therefore, the hypothesis is that RipA under different conditions and at different times binds different proteins and participates with the same function in different cell process like PG synthesis or degradation.

Experiments carried out *in vivo* show that RipA localizes at the septa and at the poles, and its activity is crucial for cell division and septation. Depletion of RipA results in long branched filament cells, and over-expression of the RipA catalytic domain causes cells to blow up and explode¹². Therefore, the activity of RipA must be highly regulated to allow cell survival. All the reported antagonistic interactions between RipA and PBP1 or RpfB and RpfE make of RipA a fundamental enzyme involved in PG synthesis and degradation during cell division in mycobacteria.

The way new peptidoglycan is coordinately synthesized and hydrolyzed during cell growth and division is a puzzle that remains unsolved in all bacteria. PG hydrolases and synthases must work in a spatially and temporally coordinated manner. The hypothesis for RipA is that during septation, RipA interacts with PBP1 and participates in the synthesis of PG between daughter cells. After the PG synthesis is completed, RipA may exchange PBP1 for an autolysin binding partner like RpfB/E. These new complexes between PG hydrolases are active on PG and split the cell wall to separate the two mature daughter cells.

The regulation of RipA activity can be inferred from this structure of the RipA₂₆₃₋₄₇₂ C-terminal catalytic domain¹³. The RipA catalytic-domain structure shows a conformation typical of an inactive enzyme. In this structure, the active-site cleft is physically blocked by an inhibitory segment that needs to be removed to allow substrate binding. It is unclear which mechanism allows RipA activation. There are two plausible hypotheses regarding the activation: the first one is RipA is a zymogen and its activity is regulated by a protease that removes the inhibitory section. The second model is that an interaction between one or more proteins contribute to conformational changes that enable the substrate to access the catalytic site. Even though the crystal structure of RipA has been solved, most aspects of how this enzyme participates to PG synthesis and degradation remain unclear.

In this chapter, I describe the search for a protein complex between PG hydrolases, using a pull down approach. We followed the idea that different classes of enzymes

may interact with each other to form active complexes. As a first step of this method, I cloned, expressed, and purified 10 hydrolases, a few from each class of enzymes, and tested these for *in vitro* interaction using GST pull down assays. Initially, I detected interaction between RpfD and Rv1478, a NlpC/P60 hydrolase, the same classes of enzymes reported previously for RipA and RipB complexes. I tested the formation of RipA – RpfB and RipB – RpfD complexes using other biochemical assays, such as native gel electrophoresis and gel filtration. We also tested the possibility of co-purifying native complexes directly from *E. coli* using multi-protein co-expression vectors. On the way to validate previous mentioned protein interactions, I solved the crystal structure of Rv1478.

2.2 Looking for protein complexes.

Mycobacterium tuberculosis encodes a high number of PG hydrolases compared to other bacteria. Although the number of hydrolases is mostly conserved in mycobacteria (Table 1), the typical Gram-positive bacterium *Staphylococcus aureus* encodes 11 hydrolases and 5 more proteins with domain of unknown function involved in cell wall hydrolysis². Gram-negative bacteria as *E. coli*, for example, encodes 23 secreted hydrolases¹⁴. *E. coli* recycles peptidoglycan, and in each generation approximately 50% of peptidoglycan is newly synthesized^{15,3}. Therefore, the high number of peptidoglycan hydrolases encoded in *E. coli* includes several hydrolases involved in PG recycling. By comparison, *Mycobacterium tuberculosis* encodes 22 hydrolases (Table 2).

Little is known, however, about peptidoglycan synthesis and degradation in mycobacteria. To study peptidoglycan regulation and activity, we produced a library of recombinant *Mtb* PG hydrolases in *E. coli*. Enzymes were cloned in different *E. coli* expression vectors. Initially, I cloned, expressed and purified a collection of 8 PG hydrolases (Table 3) (Figure 1). The peptidoglycan-hydrolase library was used for activity tests and for pull downs to detect any possible interaction between hydrolases. The activity tests on the *E. coli* peptidoglycan and the *Mycobacterium smegmatis* cell wall did not show any activity (data not shown), leading us to formulate the hypothesis that *Mtb* peptidoglycan hydrolases must be highly regulated to limit their toxicity.

To investigate potential mechanisms of hydrolase activation, we mixed PG hydrolases and assayed for interactions among them. Specifically, we tested GST-tagged Rv1477, Rv1478, Rv0024, Rv2190c, Rv1566c, Rv3915, Rv3717 and Rv3811 for interaction with RpfD tagged with HisMBP. Rv1477, Rv1478, Rv0024, Rv2190c, Rv1566c, Rv3915, Rv3717 and Rv3811, all GST-tagged, were incubated at equimolar concentration with His-MBP RpfD for 30 minutes at 4 °C in Buffer A (0.3 M NaCl, 20 mM Tris pH 8, 0.5mM TCEP, 10% glycerol). A native gel stained with Coomassie blue

showed (Figure 2) a new band for Rv1478 bound to HisMBP-RpfD. Based on the band intensities, the interaction between Rv1478 and RpfD looks stoichiometric. The apparent interaction between Rv1478 and RpfD showed the same qualitative specificity as RipA (Rv1477) and RpfB as reported by Rubin (reference). Thus, to confirm the interaction between Rv1478-RpfD and RipA-RpfB we carried out other biochemical assays to study the interaction and activity of the two complexes.

2.3 Rv1478 and RpfD interaction.

To test the interaction between Rv1478 and RpfD we isolated GTS-Rv1478 and HisMBP-RpfD by affinity chromatography from *E. coli*, and investigate, by size exclusion chromatography, any potential interaction between the two proteins. After TEV cleavage, we incubated proteins for 30 min at 4 °C at equimolar concentration in the same buffer condition describe above. Analytical size exclusion chromatography profiling showed three peaks not well solved (Figure 3). A Coomassie blue-stained denaturing polyacrylamide gel showed a very complex profile: fractions in the first peak at 8 ml contained uncleaved HisMBP-RpfD; fractions in the second peak at 11.38 ml contained three different bands, uncleaved GST-Rv1478, HisMBP and GST, and fractions in the last peak contained Rv1478. We inferred from this size exclusion elution profile that HisMBP-RpfD ran on the gel filtration column at high molecular weight, typical of insoluble and misfolded proteins. In addition, we noticed that TEV protease very inefficiently cleaved the His-MBP tag, and the small amount of HisMBP was not correlated with a band corresponding to RpfD alone. We asked why TEV was so inefficient during this reaction and why RpfD alone did not appear on the gel.

RpfD, like all the other peptidoglycan hydrolases, is secreted to the periplasm^{16,17}. All the other resuscitation promoting factors in *Mtb* encode a signal peptide to address secretion, but RpfD is the only one that does not encode signal peptide. Taken together, experimental data suggest a misfolded status for this enzyme and the missed secretion sequence, suggested a probable transmembrane domain. We

investigated RpfD amino acid sequence through TMHMM software¹⁸ for membrane domain prediction. TMHMM software confirmed the presence of a predicted transmembrane helix at the N terminus of the sequence (Figure 4). Consequently, to validate the interaction between RpfD and Rv1478, we cloned a different RpfD truncation starting after trans-membrane domain.

2.4 RpfD refolding strategy.

The new truncation of RpfD₄₈₋₁₅₄-His-Trx was completely insoluble in the cell pellet. To extract the protein from inclusion bodies¹⁹ we used strong denaturing conditions to completely unfold the protein (urea or guanidine 6M), and we developed a refolding protocol^{20,21} by decreasing the urea or guanidine concentration in the presence of a 10:1 ratio of reduced-to-oxidized glutathione. During the refolding protocol, we noticed that a very important step for complete refolding was the oxidation of 4 cysteines to disulphide bonds^{22,23}. This suggested that the disulphide bonds are essential for the correct and complete folding of this enzyme. Correct folding of the enzyme was confirmed by size exclusion chromatography (Figure 5).

Once RpfD₄₈₋₁₅₄ was refolded and soluble, we tested the interaction with Rv1478 using size exclusion chromatography. We mixed equimolar amount of RpfD₄₈₋₁₅₄ and Rv1478 and injected the sample on an analytical Superdex S75 size exclusion column. The purified proteins eluted as a single peak at 12.69 ml, but we did not observe any significant shift in elution volume between the hypothetical complex and the individual proteins (RpfD₄₈₋₁₅₄ dimer 13.05mL; Rv1478 12.65 ml) (Figure 6). The same experiment was repeated with RpfD₄₈₋₁₅₄ monomer, but in this case, we used GST-tagged Rv1478 to avoid overlaps between elution peaks corresponding to the individual proteins and the expected complex. We tested also the hypothetical interaction using native gel shift. The Coomassie blue gel did not show any shift in band between the two single proteins and the hypothetical complex (data not shown). These results were inconsistent with the results we observed initially in the

GST pull down experiments (figure 2). With these conflicting data available, we believe that the correctly folded RpfD₄₈₋₁₅₄ and Rv1478 do not form a complex *in vitro*.

2.5 RpfB and RipA interaction.

Given our contrasting results about the Rv1478 and RpfD₄₈₋₁₅₄ interaction, we tested the interaction between RpfB and RipA (Rv1477) using the same biochemical assays. Since an equimolar mixture of RpfD and Rv1478 did not show any evidence of interaction *in vitro*, we asked if the interaction between these two classes of enzymes might require a specific native conformation populated only if both proteins are co-expressed at the same time in the same expression system. For this reason, we used for this complex a different approach. We cloned both proteins in the same co-expression vectors with combinations of different tags and different truncations (Table 4) to overcome probable solubility and expression problems. We tested two different truncations of RipA fused to a strep tag (RipA-L: 43-472; RipA-S 263-472) and two different truncations of RpfB (RpfB-L 44-362 and RpfB-S 194-362) with 4 different tags (HisMBP, HisSUMO, HisTrx, HisMOCR). We transformed dual expression vectors in *E. coli*, and all the vectors containing RipA-S did not grow well (colonies were pinprick-sized or nonexistent), suggesting that the protein inhibits cell growth and the combination of RpfB-L/S with RipA-S was toxic for bacterial cells.

In contrast, cells carrying vectors containing RipA-L grew well. Based on this result, we tested for interactions of I, K, M, O plasmid combinations, but only for the combination I, we were able to get some RipA-L soluble in the supernatant. The complex was investigated by size exclusion chromatography, which did not show clear results (Figure 7).

Since most of the RipA-L was insoluble, the only way to study the interaction between RipA and RpfB was to try to troubleshoot the growth condition for the other 4 combinations with the short form of RipA. We incubated *E. coli* cells carrying A and E combination vectors at 37 °C for 24 hours to allow the few colonies to grow. These were used to inoculate small- and large-scale broth cultures. Cells grew very slowly and reached OD₆₀₀=0.6 after 10-12 hours. Although we were able to grow cells carrying both plasmids, only combination E with RipA-S strep tag and RpfB-L HisMBP tag expressed both proteins. We isolated the complex of RipA and RpfB from supernatant using affinity chromatography (Ni column) (Figure 8-A). However, we got completely different results by size exclusion chromatography, where the elution chromatogram shows two different peaks completely separated. Coomassie blue gel confirmed that no interaction between RipA and RpfB existed in the condition we were operating (Figure 8-B). Although, the two protein masses were only 15 kDa apart, RpfB ran at a higher apparent molecular mass, probably due to the elongated shape of the protein. In light of these results, we thought this interaction was not compatible with the buffer conditions used (0.1M NaCl, 0.02M Tris pH 8, 5% glycerol). For this reason, we examined the interaction between RipA and RpfB in different buffer conditions, by testing several salt concentrations and pHs. All the buffer combinations gave negative results.

We asked also whether the complex may undergo a conformational change during the execution of the experiment with the consequent disruption of its interactions. To test this idea, fractions containing both proteins eluted from the Ni column without TEV cleavage step were injected on size exclusion column. Results showed the same separated species (data not shown).

2.6 Rv1478/RipB structure.

The *Mycobacterium tuberculosis* genome encodes Rv1477 (RipA) and Rv1478 (RipB) in the same operon. RipA is a long protein with an N-terminal domain of unknown

function and a C-terminal catalytic domain. Experiments *in vivo* showed that RipA is cleaved to produce a C-terminal fragment that runs around 27 kDa¹². The catalytic domain shares a high identity and similarity in amino acid sequence with RipB (Blast alignment shows 61% identity and 72% similarity).

We solved the crystal structure of Rv1478 (Figure 9). RipB adopts a fold very similar to RipA and conserves the same catalytic triad Cys, His and Asp¹³. The crystal structure reveals an auto-inhibited native conformation with a prodomain that blocks access of the substrate to catalytic site (figure 10). The inactivating loop is conserved also in RipA, but differently packed between the two proteins: RipA shows a beta-hairpin into the lid, while RipB shows two alpha helices packed at 90 degrees. The two structures also show minor differences at the C terminus, where a loop is oriented in a different way. Analysis of Rv1478 surface reveals a hole in the body of the enzyme with an asparagine completely exposed.

Both enzymes are inactive in their native conformation and both need the movement of the N terminus to allow substrate access to the catalytic site. The activation mechanism for both proteins remains still unknown and under investigation.

2.7 Discussion.

Cell-wall hydrolases are involved in many processes of synthesis and degradation, and their activities are crucial to cell survival and mobility. How *Mycobacterium tuberculosis*, and all the other bacteria, coordinate the spatio-temporal activities of PG hydrolases to limit their toxicity is not well understood. The hypothesis proposed by Rubin is that the activities of hydrolases like RipA are regulated by interactions with other proteins; the right interaction switches the enzymes from the inactive to the active form. The interaction proposed for RipA and RpfB is very intriguing. The two cell-wall hydrolases have been proposed to synergize to control and regulate each other's activity^{8,10,12}.

We investigated with biochemical methods the potential interactions between RipA and RpfB, as well as RipB and RpfD. The results showed no interaction. Most likely, the RipB and RpfD interaction detected *in vitro* during GST pull downs is a false positive due to the misfolded status of RpfD. Quite interestingly, we detected the interaction only for RipB and not for any other hydrolases tested in the same assay. It is possible that the transmembrane domain deleted in our experiment to remove the aggregate may play a role in the interaction with RipB.

For RipA and RpfB, our experiments revealed conflicting data. Primarily, plasmids carrying both hydrolases are toxic for *E. coli*, inhibiting the growth of the cells. We found out experimentally how to grow *E. coli* only for two constructs of RipA and RpfB. However, one of these constructs does not express the proteins and the other one expresses both proteins but they do not form a complex. The hypothesis here is that *E. coli* in order to grow under these stress conditions, produces an inactive form of the complex. Alternatively, the complex may need a third component to be stable and detectable.

The RipA and RipB crystal structures validated the hypothesis that hydrolases need to regulate their activity, and in this specific case need to be activated in order to

function¹³. Both enzymes overlap well for most of the structure, except for the N-terminus where we think different interacting partners may regulate different functions within the cells.

2.8 Materials and Methods.

Rv0024 cloning, expression and purification. Oligonucleotide primers were designed to amplify nucleotide sequences corresponding to different Rv0024 (1-181) by PCR using H37Rv genomic DNA. Primer sequences contained the insertion site for the TOPO TEV vector. The PCR products were cloned in an expression vector (pDest15 Gateway) carrying a TEV cleavable N-terminal GST tag. The positive plasmid was transformed in Rosetta2(DE3)pLysS expression system.

Cells were grown at 37 °C until OD₆₀₀ 0.6 was reached, and cultures were induced with 1mM IPTG at 18 °C and shaken overnight for protein expression. The pellet was resuspended in Buffer A (300mM NaCl, 20mMTris pH 8, 10% glycerol, 0.5 mM TCEP) containing protease inhibitors. The pellet was sonicated and the lysate was centrifuged at 18000 rpm for 1 hour. Supernatant was loaded on a GST-affinity column and washed with 10 volumes of Buffer A. Protein was eluted with Buffer B (300 mM NaCl, 20 mM Tris pH 8, 0.5 mM TCEP, 20 mM reduced glutathione). The protein was dialyzed against buffer A overnight to remove glutathione. The protein was flash frozen in liquid nitrogen and stored for further experiments.

Rv1009 cloning, expression and purification. Oligonucleotide primers were designed to amplify nucleotide sequence corresponding to Rv1009 (24-362) by PCR using H37Rv genomic DNA. Primer sequences contain the insertion site for the TOPO TEV vector. The PCR product was cloned in an expression vector (pHGWA Gateway) carrying a TEV cleavable N-terminal His tag. The positive plasmid was transformed into the Rosetta2(DE3)pLysS expression system.

–

Cells were grown at 37 °C until OD₆₀₀ 0.6 was reached and cultures were induced with 1mM IPTG at 18C and left overnight for protein expression. The pellet was resuspended in Buffer A (300 mM NaCl, 20 mM imidazole pH 8, 20 mM Tris pH 8, 10% glycerol, 0.5 mM TCEP), containing protease inhibitors. The pellet was

sonicated and the lysate spun down at 18000rpm for 1 hour. Coomassie blue gel (data not shown) for lysate, pellet and supernatant showed that the expected band around 40 kDa was present in the lysate and in the pellet but not in the supernatant. The protein was insoluble and we did not proceed to affinity purification from the supernatant. The pellet was flash frozen by liquid nitrogen and stored for further experiments.

Rv1477 cloning, expression and purification. Oligonucleotide primers were designed to amplify nucleotide sequences corresponding to different truncations of Rv1477 (41-472 and 263-472) by PCR using H37Rv genomic DNA. Primer sequences contain the insertion site for the TOPO TEV vector. The PCR products were cloned in an expression vector (pDest15 Gateway) carrying a TEV cleavable N-terminal GST tag. The positive plasmid was transformed into the Rosetta2(DE3)pLysS expression system.

Cells were grown at 37 °C until OD₆₀₀ 0.6 was reached, then cultures were induced with 1mM IPTG at 18C and left overnight for protein expression. The pellet was re-suspended in Buffer A (300mM NaCl, 20mMTris pH 8, 10% glycerol, 0.5 mM TCEP), containing protease inhibitors cocktails. The pellet was sonicated and the lysates spun down at 18000rpm for 1 hour. Supernatant was loaded on a GST-affinity column and then washed with 10 volumes of Buffer A. Proteins were eluted with Buffer B (300 mMNaCl, 20mMTris pH 8, 0.5 mM TCEP, 20 mM reduced glutathione). The protein was dialyzed against buffer A overnight to remove glutathione. The proteins were flash frozen in liquid nitrogen and stored for further experiments.

Rv1566c cloning, expression and purification. Oligonucleotides primers were designed to amplify nucleotide sequences corresponding to Rv1566c (29-170) by PCR using H37Rv genomic DNA. Primer sequences contained the insertion for the TOPO TEV vector. The PCR products were then cloned in an expression vector (pDest15 Gateway) carrying a TEV cleavable N terminus GST tag. The positive plasmid was then transformed in Rosetta2(DE3)pLysS expression system.

Cells were grown at 37 °C until OD₆₀₀ 0.6 was reached, then cultures were induced with 1mM IPTG at 18C and left overnight for protein expression.

The pellet was re-suspended in Buffer A (300mM NaCl, 20mMTris pH 8, 10% glycerol, 0.5 mM TCEP), containing protease inhibitors cocktails. The pellet was sonicated and the lysate spun down at 18000rpm for 1 hour. Supernatant was loaded on a GST-affinity column and then washed with 10 volumes of Buffer A. The protein was eluted with Buffer B (300 mMNaCl, 20mMTris pH 8, 0.5 mM TCEP, 20 mM reduced glutathione). The protein was dialyzed against buffer A overnight to remove glutathione. The protein was flash frozen in liquid nitrogen and stored for further experiment.

Rv2190c cloning, expression and purification. Oligonucleotides primers were designed to amplify nucleotide sequences corresponding to Rv2190c (33-385) by PCR using H37Rv genomic DNA. Primer sequences contained the insertion for TOPO TEV vector. The PCR products were then cloned in an expression vector (pDest15 Gateway) carrying a the TEV cleavable N terminus GST tag. The positive plasmid was then transformed in Rosetta2(DE3)pLysS expression system.

Cells were grown at 37 °C until OD₆₀₀ 0.6 was reached, then cultures were induced with 1mM IPTG at 18C and left overnight for protein expression.

The pellet was re-suspended in Buffer A (300mM NaCl, 20mMTris pH 8, 10% glycerol, 0.5 mM TCEP), containing protease inhibitors cocktails. The pellet was sonicated and the lysate spun down at 18000rpm for 1 hour. Supernatant was loaded on a GST-affinity column and then washed with 10 volumes of Buffer A. Protein was eluted with Buffer B (300 mMNaCl, 20mMTris pH 8, 0.5 mM TCEP, 20 mM reduced glutathione). The protein was dialyzed against buffer A overnight to remove glutathione. The protein was flash frozen in liquid nitrogen and stored for further experiment.

Rv3915 cloning, expression and purification. Oligonucleotides primers were designed to amplify nucleotide sequences corresponding to Rv3915 (1-406) by PCR using H37Rv genomic DNA. Primer sequences contained the insertion for the TOPO

TEV vector. The PCR products were then cloned in an expression vector (pDest15 Gateway) carrying a TEV cleavable N terminus GST tag. The positive plasmid was then transformed in Rosetta2(DE3)pLysS expression system.

Cells were grown at 37 °C until OD₆₀₀ 0.6 was reached, then cultures were induced with 1mM IPTG at 18C and left overnight for protein expression.

The pellet was re-suspended in Buffer A (300mM NaCl, 20mMTris pH 8, 10% glycerol, 0.5 mM TCEP), containing protease inhibitors cocktails. The pellet was sonicated and the lysate spun down at 18000rpm for 1 hour. Supernatant was loaded on a GST-affinity column and then washed with 10 volumes of Buffer A. The protein was eluted with Buffer B (300 mM NaCl, 20mMTris pH 8, 0.5 mM TCEP, 20 mM reduced glutathione). The protein was dialyzed against buffer A overnight to remove glutathione. The protein was flash frozen in liquid nitrogen and stored for further experiment.

Rv3717 cloning, expression and purification. Oligonucleotides primers were designed to amplify nucleotide sequences corresponding to Rv3717 (25-241) by PCR using H37Rv genomic DNA. Primer sequences contained the insertion for the TOPO TEV vector. The PCR products were then cloned in an expression vector (pDest15 Gateway) carrying a TEV cleavable N terminus GST tag. The positive plasmid was then transformed in Rosetta2(DE3)pLysS expression system.

Cells were grown at 37 °C until OD₆₀₀ 0.6 was reached, then cultures were induced with 1mM IPTG at 18C and left overnight for protein expression.

The pellet was re-suspended in Buffer A (300mM NaCl, 20mMTris pH 8, 10% glycerol, 0.5 mM TCEP), containing protease inhibitors cocktails. The pellet was sonicated and the lysate spun down at 18000rpm for 1 hour. Supernatant was loaded on a GST-affinity column and then washed with 10 volumes of Buffer A. Protein was eluted with Buffer B (300 mMNaCl, 20mMTris pH 8, 0.5 mM TCEP, 20 mM reduced glutathione). The protein was dialyzed against buffer A overnight to remove glutathione. The protein was flash frozen in liquid nitrogen and stored for further experiment.

Rv3811 cloning, expression and purification. Oligonucleotides primers were designed to amplify nucleotide sequences corresponding to Rv3811 (1-539) by PCR using H37Rv genomic DNA. Primer sequences contained the insertion for the TOPO TEV vector. The PCR products were then cloned in an expression vector (pDest15 Gateway) carrying a TEV cleavable N terminus GST tag. The positive plasmid was then transformed in Rosetta2(DE3)pLysS expression system.

Cells were grown at 37 °C until OD₆₀₀ 0.6 was reached, then cultures were induced with 1mM IPTG at 18C and left overnight for protein expression.

The pellet was re-suspended in Buffer A (300mM NaCl, 20mMTris pH 8, 10% glycerol, 0.5 mM TCEP), containing protease inhibitors cocktails. The pellet was sonicated and the lysate spun down at 18000rpm for 1 hour. Supernatant was loaded on a GST-affinity column and then washed with 10 volumes of Buffer A. Protein was eluted with Buffer B (300 mMNaCl, 20mMTris pH 8, 0.5 mM TCEP, 20 mM reduced glutathione). The protein was dialyzed against buffer A overnight to remove glutathione. The protein was flash frozen in liquid nitrogen and stored for further experiment.

Rv2389c cloning, expression and purification. Oligonucleotides primers were designed to amplify nucleotide sequences corresponding to Rv2389c (1-1544) by PCR using H37Rv genomic DNA. Primer sequences contained the insertion for the TOPO TEV vector. The PCR products were then cloned in an expression vector (pHMGWA Gateway) carrying a TEV cleavable N terminus GST tag. The positive plasmid was then transformed in Rosetta2(DE3)pLysS expression system.

Cells were grown at 37 °C until OD₆₀₀ 0.6 was reached, then cultures were induced with 1mM IPTG at 18C and left overnight for protein expression.

The pellet was resuspended in Buffer A (300 mM NaCl, 20 mM imidazole pH 8, 20 mM Tris pH 8, 10% glycerol, 0.5 mM TCEP) containing protease inhibitors. The pellet was sonicated, and the lysate centrifuged at 18000rpm for 1 hour. Supernatant was loaded onto a Ni-affinity column and washed with 10 volumes of Buffer A. Protein was eluted with Buffer B (300 mM NaCl, 20 mM Tris pH 8, 0.5 mM

TCEP, 300 mM imidazole). The protein was dialyzed against buffer A overnight to remove the imidazole. During dialysis, the tag cleavage reaction was performed using TEV protease.

A second affinity purification using a Ni-affinity column was performed to remove the tag. The protein once concentrated was injected for a gel filtration step for further purification. Gel filtration elution shows a peak at high molecular weight typical of misfolded proteins. All the attempts to remove aggregate, like high salt and/or dialysis against 1 M urea were unsuccessful (data not shown).

The RpfD sequence was analyzed using several computer programs to explore the hypothetical transmembrane domains. Results indicated that RpfD has a transmembrane helix (20-40). A new construct starting at residue 48 was designed. The PCR product was cloned in a pDest-59 (Novagen) carrying an N-terminal His-Trx tag. RpfD-Trx was not soluble, and it accumulated as an insoluble protein in the pellet. A strategy of refolding was developed. The pellet was completely solubilized in 6M urea by sonication, centrifuged for 1 hour at 18000 rpm, and the supernatant was loaded to a Ni-affinity column. All the starting purification steps were carried out in 6M urea. The refolding protocol consists of many steps of dialysis where the concentration of urea was slowly lowered. The first step was dialysis against 4 M urea, 300mM NaCl, 20mM Tris pH 8, 10% glycerol. This step is followed by another one with a buffer in 2 M urea and a redox system (1 mM reduced glutathione, 0.1M oxidized glutathione) to allow the formation of two disulphide bonds essential for RpfD folding. Urea was completely removed and a gel filtration purification step was used to check the folding status of the protein and also as the last step of purification. This refolding strategy led to a folded protein that behaved as a dimer.

A different strategy of refolding was developed. In this case, instead of performing the refolding steps in a dialysis bag using buffer with different concentrations of urea, a Ni-affinity column was used as a fixed support where the protein was bound during the refolding process to avoid domain swapping. The second strategy of

refolding was carried out using a decreasing gradient of buffer B at high concentration of Guanidine-HCl (6 M Gu-HCl, 300 mM NaCl, 20 mM imidazole, 20mM Tris pH8, 10% glycerol) and an increasing gradient of buffer A containing 300 mM NaCl, 20 mM imidazole, 20 mM Tris pH8, 10% glycerol, 10 mM of reduced glutathione and 1mM of oxidized glutathione. The protein was eluted using buffer Ni-B (300 mM NaCl, 20 mM Tris pH 8, 10% glycerol, 300 mM imidazole) dialyzed in the same buffer to remove imidazole. During dialysis, TEV protease cleavage was performed. The gel filtration purification step showed a peak typical of a protein monomer.

Rv1478, cloning, expression, and purification. Oligonucleotide primers were designed to amplify nucleotide sequences corresponding to Rv1478 (31-242) by PCR using H37Rv genomic DNA. Primer sequences contained the insertion for the TOPO TEV vector. The PCR products were then cloned in an expression vector (pDest15 Gateway) carrying a TEV cleavable N terminus GST tag. The positive plasmid was then transformed in Rosetta2(DE3)pLysS expression system.

Cells were grown at 37 °C until OD₆₀₀ 0.6 was reached, then cultures were induced with 1mM IPTG at 18C and left overnight for protein expression. The pellet was re-suspended in Buffer A (300mM NaCl, 20mMTris pH 8, 10% glycerol, 0.5 mM TCEP). The buffer contains protease inhibitors cocktails. The pellet was sonicated and the lysate spun down at 18000rpm for 1 hour. Supernatant was loaded on a GST-affinity column and then washed extensively with Buffer A. Protein was eluted with Buffer B (300 mMNaCl, 20mMTris pH 8, 0.5 mM TCEP, 20 mM reduced glutathione). The protein was dialyzed over night in the same buffer condition and (300 mM NaCl, 20 mMTris pH 8, 0.5 mM TCEP 10% glycerol) to remove glutathione. During dialysis TEV protease cleavage was performed. A second affinity purification on a glutathione column was used to remove the GST tag. Once the tag was separated from Rv1478, the protein was concentrated and injected for a further purification using gel filtration (data not shown). This strategy of purification gave a single peak for Rv1478, but most of the fractions contained different amounts of Rv1478 and

tag. A different strategy of purification was attempted. Fractions containing Rv1478 and GST were combined and dialyzed against a low salt buffer (30 mM NaCl, 20 mM Tris pH 8, 0.5 mM TCEP, 10% glycerol) and passed through an HQ (ion exchange) column. Using this purification approach, Rv1478 flowed through the column, and the GST tag was retained.

Rv1478 Crystallization and structure determination. Preliminary Rv1478 crystals were obtained by hanging drop vapor diffusion at 18 °C from a 1:1 mixture of 23 mg/mL protein with 8% 2-propanol, 16% (w/v) PEG 3000, 50 mM NaCitrate pH 5.5. Diffraction quality crystals were obtained by hanging drop vapor diffusion at 18 °C by seeding 1:1 mixture of 23 mg/mL protein with 8% 2-propanol, 16% (w/v) PEG 3000, 50 mM NaCitrate pH 5.5. Crystals were immersed in mother liquor containing 15% glycerol, mounted, and flash frozen in liquid N₂. Diffraction data were collected at the Lawrence Berkeley National Laboratory Advanced Light Source Beamline 8.3.1²⁴. The PHENIX²⁵ software suite was used for model building by molecular replacement using as model 3NE0 homolog in Protein Data Bank (PDB). Cycles of refinement were performed by with PHENIX²⁵. Images and structural alignments were generated using Chimera²⁶.

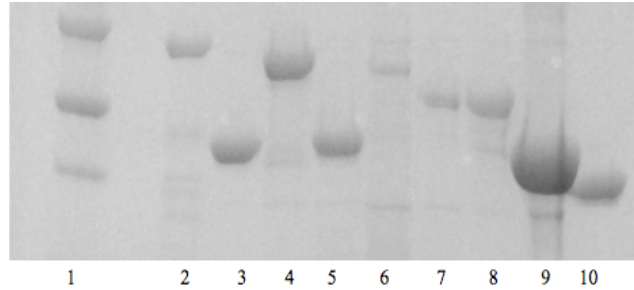
GST pull down experiments. GST-tagged Rv1477, Rv1478, Rv0024, Rv2190c, Rv1566c, Rv3915, Rv3717 and Rv3811 were tested for interaction with RpfD HisMBP. The pull down experiment was carried out in buffer A (0.3 M NaCl, 20 mM Tris pH 8, 0.5 mM TCEP, 10% glycerol). 100 µL of each GST-tagged protein was bound on glutathione resin and the surplus of unbound proteins washed away. 200 µL of RpfD HisMBP was added to each protein bound on the GST-affinity resin. The mixture was gently rotated at 4 °C for 30 min. After the supernatant was removed, the resin was washed with 10 volumes of buffer A. Samples were boiled in SDS loading dye for 10 min, and 10 µL of each supernatant was run on a denaturing polyacrylamide gel. Coomassie blue stain showed a new band at the molecular weight of RpfD HisMBP in the Rv1478 sample.

RpfB-Rv1477: cloning, expression, purification. RpfB and RipA were cloned in a polisystronic plasmid (2E- <http://www.addgene.org>.) with a combination of 4 different tags for RpfB (6HisMBP; 6HisSUMO; 6HisMocR; 6HisTrx) and a single tag for Rv1477 (strep). For both proteins, full-length sequences and truncations containing the catalytic domain were tested (see Table 4).

Cells were grown at 37 °C until the OD₆₀₀ reached 0.6 and then induced by 1 mM IPTG at 16 °C for 8 hours. Cells were lysed in 100 mM NaCl, 20 mM Tris pH 8, 0.5 mM TCEP, 20 mM imidazole pH 8, 5% glycerol), and the supernatant was loaded onto a Ni-affinity column, washed and eluted with 100 mM NaCl, 300mM imidazole, 20mM Tris pH 8, 0.5 mM TCEP, 5% glycerol. The proteins were dialyzed against a redox system to form disulphide bonds critical to the folding and stability of rpfB (dialysis buffer: 100 mMNaCl, 20mMTris pH 8, 0.5 mM TCEP, 5% glycerol, 1mM reduced glutathione-0.1mM oxidated glutathione). The TEV protease reaction to remove the tag was performed during the dialysis step. The two proteins after the rebinding step were concentrated and injected onto an S200 gel filtration to study the behavior as a complex. Purifications for the complex at pH 7 and 5 in the same buffer condition were performed.

2.9 Figures.

Figure 1. Library of 8 peptidoglycan Hydrolases expressed in *E. coli*.



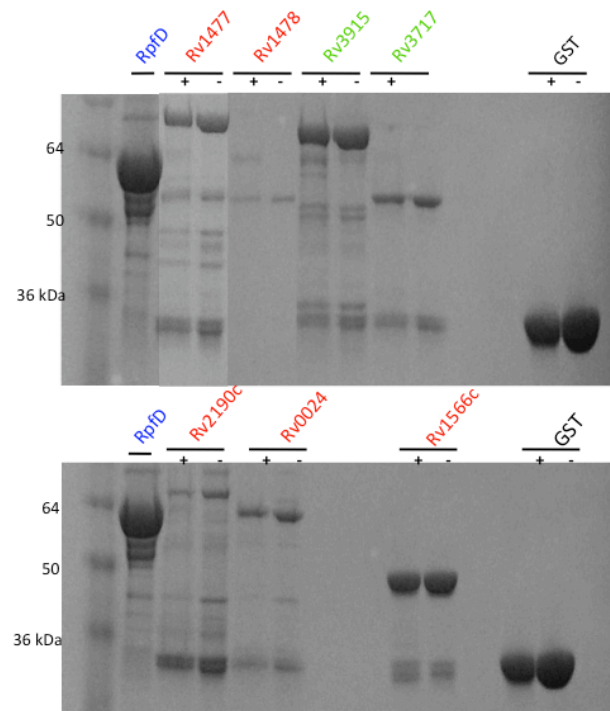
Peptidoglycan hydrolases expressed in *E. coli* and purified by affinity chromatography.

1-Protein ladder from the top to the bottom 64 kDa, 50 kDa and 36 kDa.

2-Rv1477, 3-Rv1478, 4-Rv3915, 5-Rv3717, 6-Rv2190c, 7-Rv0024, 8-Rv2389c,

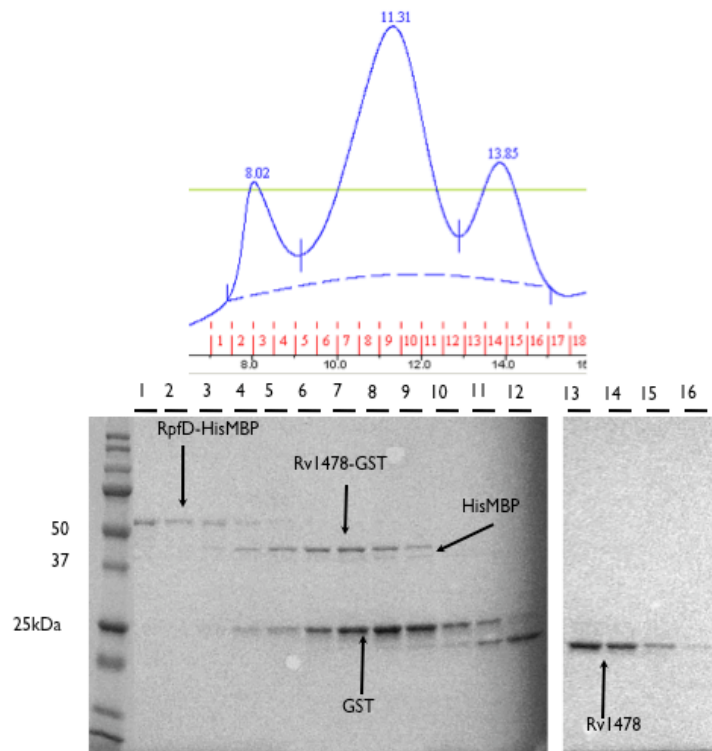
9-Rv1009, 10-Rv1566c.

Figure 2. GST pull downs.



Coomassie blue stained gel of GST pull downs. Enzymes highlighted in blue are transglycosylases (RpfD), enzymes highlighted in red are peptidases, and enzymes in green are amidases. The GST pull down experiments were carried out in 300 mM NaCl, 20 mM Tris pH 8, 10% glycerol and 0.5 mM TCEP. RpfD-HisMBP was mixed with other enzymes on a GST-affinity resin. The only sample that produced evidence for an apparent interaction was Rv1478.

Figure 3. Size exclusion chromatography for Rv1478 and RpfD.

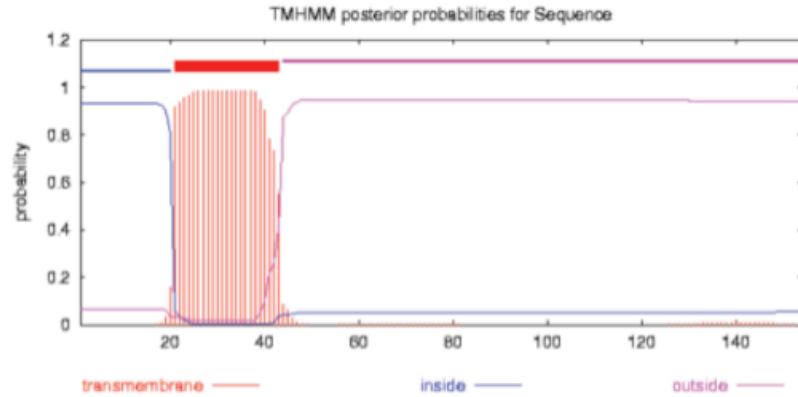


Exploratory size exclusion chromatography elution for Rv1478-RpfD complex after TEV protease cleavage. As shown by the Coomassie blue-stained gel, RpfD His-MBP eluted at 8.02 mL, at high molecular weight elution typical of misfolded protein. GST dimer, uncleaved Rv1478-GST and His-MBP eluted all in a large peak at 11.31 mL. Rv1478 by itself eluted at 13.85 mL.

Figure 4. RpfD transmembrane helix prediction.

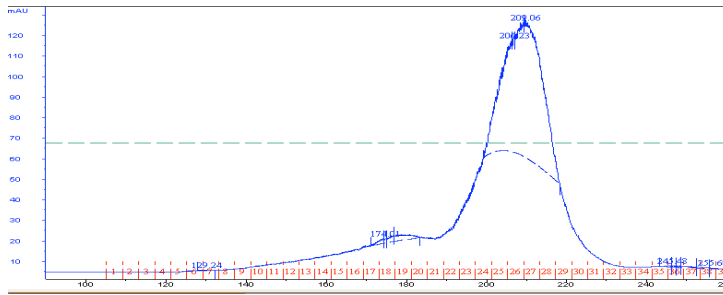
RpfD transmembrane helix prediction.

No	N terminal	Transmembrane region	C terminal	Type	Lenght
1	20	RIVCTVFIETAVVATMFVALLGLST	43	primary	23



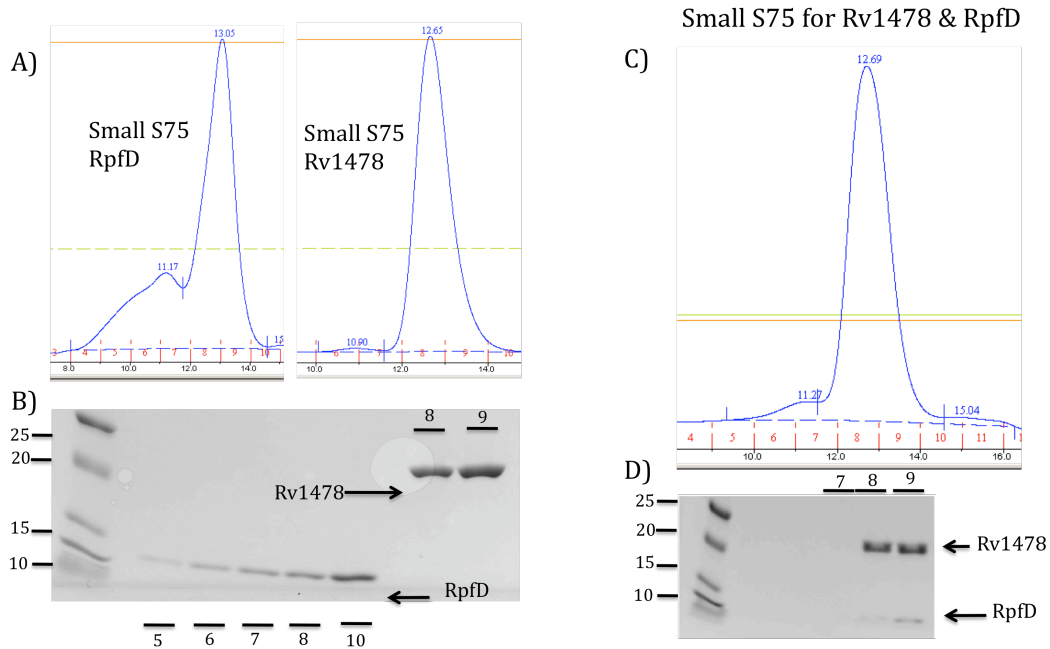
The RfpD sequence was analyzed using TMHMM software. Results show a single predicted TM helix in the amino acid sequence of RpfD.

Figure 5. Size exclusion chromatography of RpfD.



After refolding, RpfD runs as a monomer on a size exclusion column (Superdex S75) in 300 mM NaCl, 20mM Tris pH8 and 10% glycerol.

Figure 6. RpfD-Rv1478 complex investigated by size exclusion chromatography.



We used size exclusion chromatography to investigate the formation of a RpfD-Rv1478 complex.

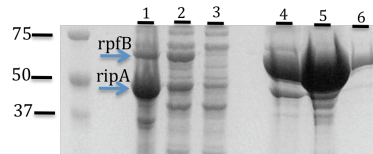
A) Elution volume for RpfD and Rv1478 alone;

B) Coomassie blue-stained gel: RpfD runs around 15 kDa and Rv 1478 around 20 kDa.

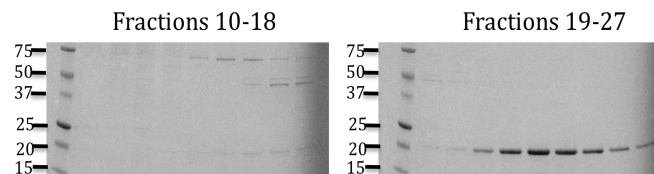
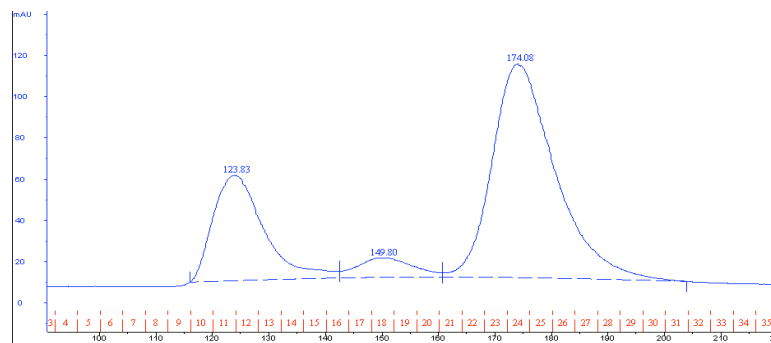
C), D) Elution volume for equimolar mixture of Rv1478 and RpfD and Coomassie blue-stained gel. Even though it is possible to observe co-elution for both proteins, no volume shift it is observed for the complex. The elution volumes for both proteins are overlapped. RpfD eluted at higher molecular weight because it probably has an elongated shape, like RpfB.

Figure 7. Complex I: RipA-L and RpfB-S HisMBP.

A



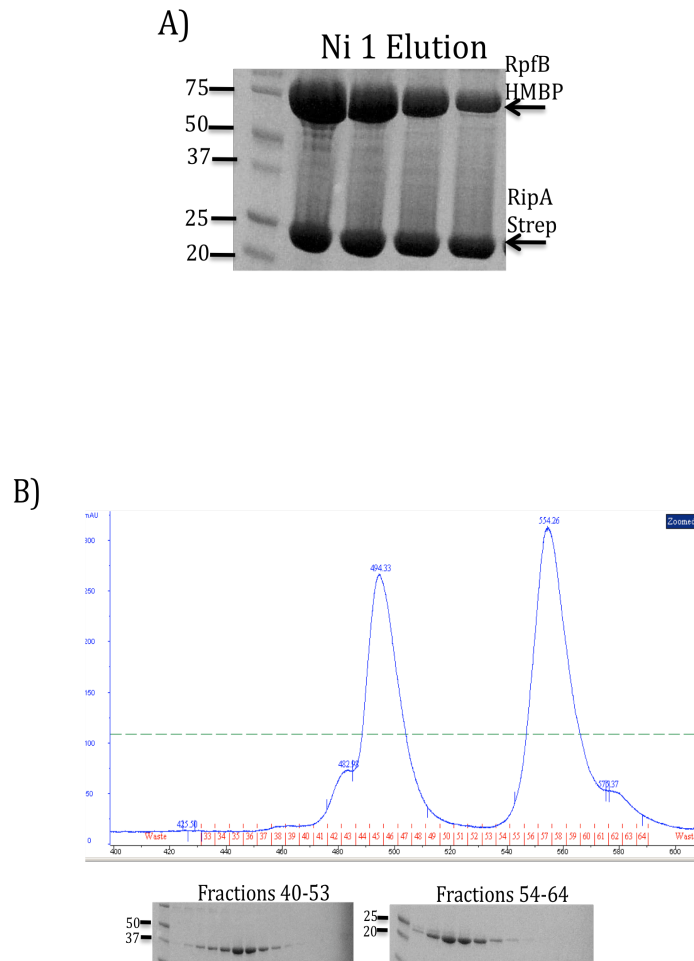
B



A) Lanes 1, 2, and 3 are the lysate, supernatant and pellet. Lanes 4-6 show the Ni-affinity elution. RipA-L is mostly insoluble in the cell pellet, and only a little amount binds to the Ni column in form of complex. In addition, gel bands for the two proteins do not show a stoichiometric ratio.

B) Size exclusion chromatography of RipA-L and RpfB-S. The first peak at 123.83 mL contains a protein of around 75 kDa (probably a contaminant); the second peak at 149.50 mL shows two bands. The upper band is RipA-L and the lower band is RpfB-S. The last peak 174.08 mL contains RpfB-S.

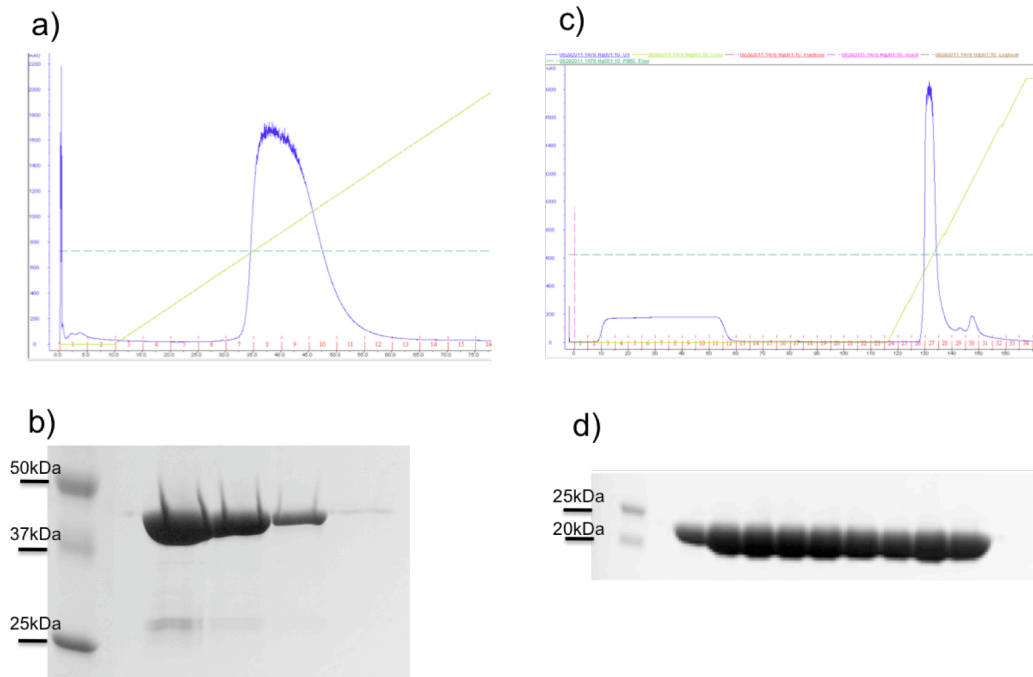
Figure 8. RipA-RpfB complex investigated by size exclusion chromatography.



A) Ni-affinity chromatography elution. Both proteins RipA-strep and RpfB-HisMBP were co-isolated during the first step of the purification.

B) Size exclusion chromatography and Coomassie blue-stained gel showing the two proteins run at different volumes and are well separated.

Figure 9. Strategy of purification of Rv1478.



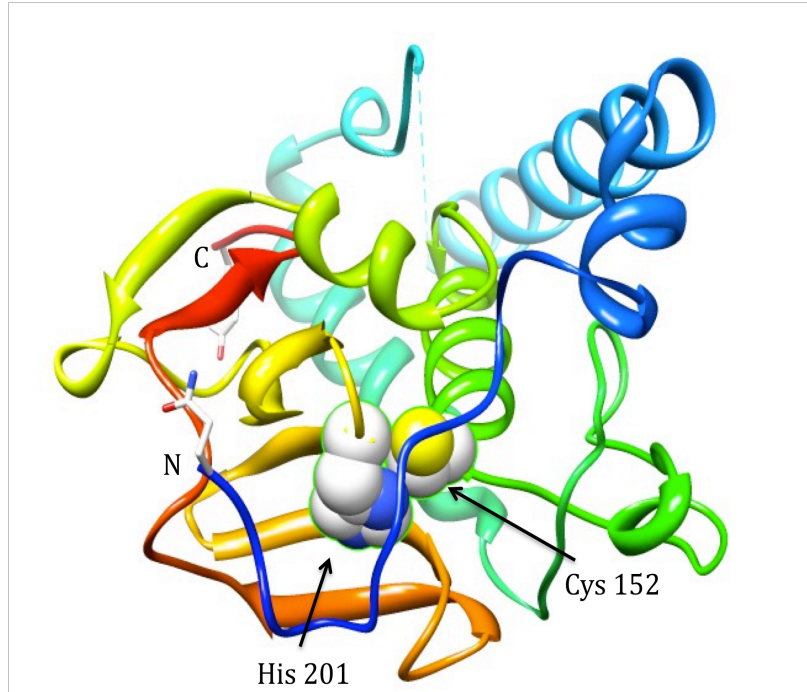
Rv1478 was purified by affinity chromatography in 300 mM NaCl, 20 mM Tris pH 8, 0.5 mM TCEP.

a, b) GST column elution for Rv1478 with GST tag and Coomassie blue-stained gel for the elution fractions.

c) ion exchange column profiling for Rv1478 after TEV protease cleavage

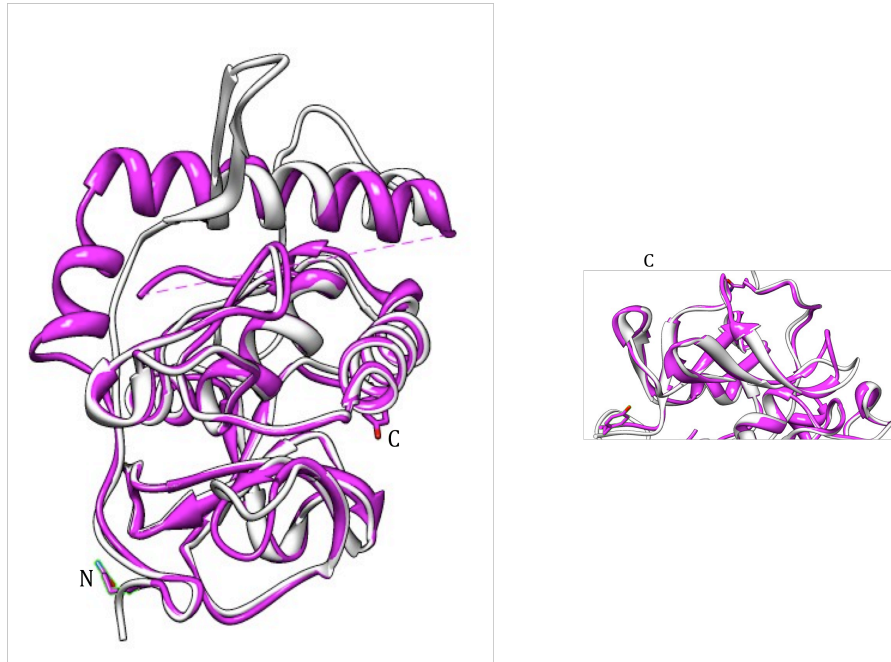
d) Coomassie blue-stained gel for flow through fractions 3-11.

Figure 10. Crystal structure of RipB (Rv1478).



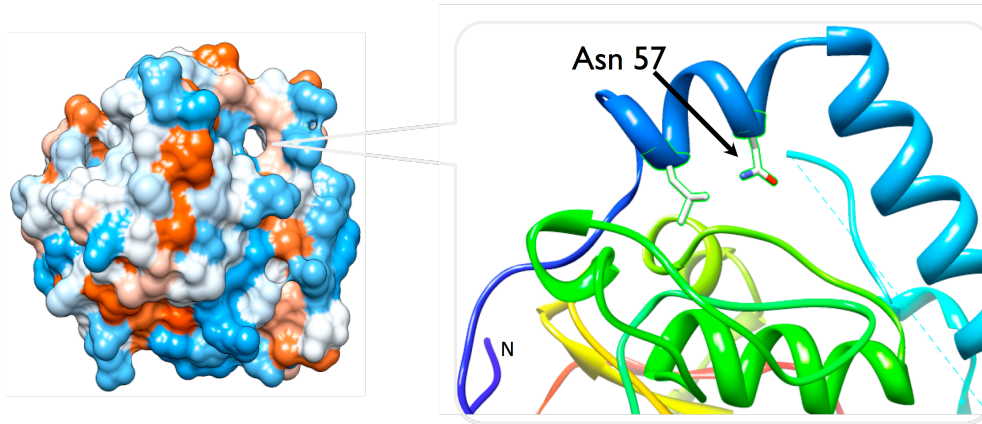
Ribbon diagram of RipB crystal structure. Catalytic Cys and His are highlighted in spheres. The N-terminus blocks substrate access to the catalytic site.

Figure 11. Superimposition of RipA and RipB.



RipA (gray) and RipB (purple) are similar in structure except for the N-terminus (top). The inactivating loop is differently packed, forming a pair of helices RipB and a β -hairpin in RipA.

Figure 12. View of RipB surface.



Rv1478 surface showing a hole in the enzyme body, with Asn57 completely exposed. The Asn is thought to have a role in the interaction with another protein or a signaling molecule, switching the enzyme from the inactive to active form by a movement of the lid (N terminus).

2.10 Tables.

Table 1. Comparison of the number of peptidoglycan hydrolases encoded in *Mycoabaterium tuberculosis*, *Mycoabaterium avium*, *Mycoabaterium abscessus*, *Mycoabaterium leprae*.

Enzymes/species	<i>M. tuberculosis</i>	<i>M. Avium</i>	<i>M. Abscessus</i>	<i>M. Leprae</i>
Amidases	4	4	4	2
Peptidases	10	9	9	6
Muramidases	8	9	7	3

Table 2. *Mycobacterium tuberculosis* peptidoglycan hydrolases. Peptidoglycan hydrolases were identified using a hidden Markov algorithm and classified by Pfam family.

	Protein name	Gene name	PFAM	Essential
I. N-acetylmuramyl-L-alanine amidases		Rv3717	Amidase_3	
	cwIM	Rv3915	Amidase_3	v
		Rv3811	Amidase_2	
		Rv3594	Amidase_2	
II. D-ala-DAP-endopeptidases		Rv3627c	Peptidase_S13	v
	dacB2	Rv2911	Peptidase_S11	
	dacB1	Rv3330		
	LpqR	Rv0838	Peptidase_M15	
	LpqF	Rv3593		v
III. D-Glu-DAP-endopeptidases	RipA	Rv1477	NLPC_P60	v
	RipB	Rv1478	NLPC_P60	
		Rv1566c	NLPC_P60	
		Rv2190c	NLPC_P60	
		Rv0024	NLPC_P60	
IV. Glycosydases		Rv1230c	SLT	
		Rv3896c	SLT	
	LpqU	Rv1022	SLT	
	RpfA	Rv0867c	Transglycosylase	
	RpfB	Rv1009		
	RpfC	Rv1884c		
	RpfD	Rv2389c		
	RpfE	Rv2450c		

Table 3. *Mtb* genome notation number, predicted signal peptide, clone truncation, tag and expression vectors.

Gene Name	SP	Clone truncation	Tag	Expression Vector
Rv0024	No	1-281 - full length	GST,	pDest15,
Rv1009	Yes	24-362 –no leader	His	pHGWA
Rv1477	Yes	41-472 – no leader	GST,	pDest15,
Rv1478	Yes	32-241 – no leader	GST	pDest15,
Rv1566c	Yes	29-170 – no leader, no tail	GST	pDest15,
Rv2190c	Yes	33-385 - no leader	GST	pDest15
Rv2389c	No	1-154 full length	HisMBP	pHMGWA
Rv3915	No	1-406 - full length catalytic domain	GST,	pDest15
Rv3717	Yes	25-241- no leader	GST,	pDest15
Rv3811	no	1-539 - full length	GST	pDest15

Table 4. RpfB-RipA coexpression cloning combinations.

	Rv1477	Rv1009
A	Short-strep	Short-MPB
B	Short-strep	Short-mOCR
C	Short-strep	Short-Sumo
D	Short-strep	Short-Thioredoxin
E	Short-strep	Long-MBP
F	Short-strep	Long-mOCR
G	Short-strep	Long-Sumo
H	Short-strep	Long-Thioredoxin
I	Long-strep	Short-MPB
J	Long-strep	Short-mOCR
K	Long-strep	Short-Sumo
L	Long-strep	Short-Thioredoxin
M	Long-strep	Long-MBP
N	Long-strep	Long-mOCR
O	Long-strep	Long-Sumo
P	Long-strep	Long-Thioredoxin

Polycistronic Systems with 4 possible combinations

- 1) RipA (43-472) – RpfB (44- 362);
- 2) RipA (43-472) – RpfB (194-362)
- 3) RipA (262-472) – RpfB (44- 362);
- 4) RipA (262-472) - RpfB (194-362).

Table 5. Blast alignment for RipA catalytic domain (Sbjct) and Rv1478 (Query).

[GENE ID: 886541 Rv1477](#) | invasion protein [Mycobacterium tuberculosis H37Rv]
 (10 or fewer PubMed links)

Score = 253 bits (647), Expect = 1e-67, Method: Compositional matrix adjust.
 Identities = 125/208 (61%), Positives = 149/208 (72%), Gaps = 0/208 (0%)

```

Query  34  GQWDPTLPALVSAGAPGDPLAVANASLQATAQATQTTLDDLGRQFLGGLGINLGGPAASAP  93
        G WDP TLP + SA  PGDP+AV N  L  +A + Q T ++GR+FL  LGI
Sbjct  265  GLWDPTLPMIPSANIPGDPIAVVNQVLGISATSAQVTANMGRKFLEQLGILQPTDTGITN  324
        * ***** + **  ***** *  *  +* + + + +*****  ***

Query  94  SAATGASRIPRANARQAVEYVIRRAGSQMGVPYSWGGSLSQGPSKGVDSGANTVGFDCS  153
        + A +  RIPR  RQA EYVIRR  SQ+GVPYSWGGS+  GPSKG+DSGA  TVGFDCS
Sbjct  325  APAGSAQGRIPRVYGRQASEYVIRRGMSQIGVPYSWGGSNAAGPSKIDSGAGTVGFDCS  384
        + * +  ****  *** *****  ****+*****+  *****+*****  *****

Query  154  GLVRYAFAGVGVLIIPRFSGDQYNAGRHVPPAEAKRGDLIFYGPGGQHVTLYLGNQMLE  213
        GLV Y+FAGVG+ +P +SG QYN GR +P ++ +RGD+IFYGP G QHVT+YLGNGQMLE
Sbjct  385  GLVLYSFAGVGIKLPHYSGSQYNLGRKIPSSQMRRGDVIFYGPNGSQHVTTIYLGNGQMLE  444
        *** *+*****+ +* +** *** ** +* ++ +*****+*****+*****

Query  214  ASGSAGKVTVSPVRKAGMTPFVTRIEY  241
        A  KV V+PVR AGMTP+V R IEY
Sbjct  445  APDVGLKVRVAPVRTAGMTPYVVRYIEY  472
        *  ** *+**** *****+* + ***
  
```

RipB data collection	
Space group	P6 ₁
Cell dimensions	<i>a</i> , <i>b</i> , <i>c</i> (Å) 92.532, 92.532, 54.064 α , β , γ (°) 90, 90, 120
Resolution (Å)	1.642
Number of molecules in asymmetric unit	1
Refinement	
R-work	0.18
R-free	0.20
Ramachandran outliers	0% (0.2%)
Ramachandran favored	98% (98%)
Rotamer outliers	3% (1%)
C-beta outliers	0
Overall score	1.75

2.11 References.

-
- ¹ Typas A, Banzhaf M, Gross CA, Vollmer W. (2011). From the regulation of peptidoglycan synthesis to bacterial growth and morphology. *Nat Rev Microbiol.* , *10(2)*, 123-36.
 - ² Layec S, Decaris B, Leblond-Bourget N. (2008). Diversity of Firmicutes peptidoglycan hydrolases and specificities of those involved in daughter cell separation. *Res Microbiol.* , *159(7-8)*, 507-15.
 - ³ Park JT, Uehara T. (2008). How bacteria consume their own exoskeletons (turnover and recycling of cell wall peptidoglycan). *72(2)*, 211-27.
 - ⁴ Vollmer W, Joris B, Charlier P, Foster S. (2008). Bacterial peptidoglycan (murein) hydrolases. *FEMS Microbiol Rev.* , *32(2)*, 259-86.
 - ⁵ Uehara T, Bernhardt TG. (2011). More than just lysins: peptidoglycan hydrolases tailor the cell wall. *Curr Opin Microbiol.* , *14(6)*, 698-703.
 - ⁶ Yang DC, Tan K, Joachimiak A, Bernhardt TG. (2012). A conformational switch controls cell wall-remodelling enzymes required for bacterial cell division. *Mol Microbiol.* , *85(4)*, 768-81.
 - ⁷ Morlot C, Uehara T, Marquis KA, Bernhardt TG, Rudner DZ. (2010). A highly coordinated cell wall degradation machine governs spore morphogenesis in *Bacillus subtilis*. *24(4)*, 411-22.
 - ⁸ Hett EC, Chao MC, Rubin EJ. (2010). Interaction and modulation of two antagonistic cell wall enzymes of mycobacteria. *LoS Pathog.* , *6(7)*, 1001020.
 - ⁹ Abanes-De Mello A, Sun YL, Aung S, Pogliano K. (2002). A cytoskeleton-like role for the bacterial cell wall during engulfment of the *Bacillus subtilis* forespore. *Genes Dev.* , *16(24)*, 3253-64.
 - ¹⁰ Hett EC, Chao MC, Deng LL, Rubin EJ. (2008). A mycobacterial enzyme essential for cell division synergizes with resuscitation-promoting factor. *PLoS Pathog.* , *4(2)*, 1000001.
 - ¹¹ Hett EC, Chao MC, Steyn AJ, Fortune SM, Deng LL, Rubin EJ. (2007). A partner for the resuscitation-promoting factors of *Mycobacterium tuberculosis*. . *66(3)*, 658-68.
 - ¹² Michael C. Chao, Karen J. Kieser¹, Shoko Minami, Daniela Mavrici, Bree B. Aldridge, Sarah M. Fortune, Tom Alber, and Eric J. Rubin. (n.d.). Protein interactions and proteolytic activation of the hydrolase RipA regulate septal resolution in *Mycobacterium tuberculosis*. *manuscript* .
 - ¹³ Ruggiero A, Marasco D, Squeglia F, Soldini S, Pedone E, Pedone C, Berisio R. (2010). Structure and functional regulation of RipA, a mycobacterial enzyme essential for daughter cell separation. *Structure* , *18(9)*, 1184-90.
 - ¹⁴ van Heijenoort J. (2011). Peptidoglycan hydrolases of *Escherichia coli*. *Microbiol Mol Biol Rev* , *75(4)*, 636-63.
 - ¹⁵ Goodell E. W. (1985). Recycling of murein by *Escherichia coli*. *J. Bacteriol.* , *163*, 305–310.
 - ¹⁶ Cole ST, Brosch R, Parkhill J, Garnier T, Churcher C, Harris D, Gordon SV, Eiglmeier K, Gas S, Barry CE 3rd, Tekaia F, Badcock K, Basham D, Brown D, Chillingworth T, Connor R, Davies R, Devlin K, Feltwell T, Gentles S, Hamlin N, Holroyd S, Hornsby T,

Jage. (1998). Deciphering the biology of *Mycobacterium tuberculosis* from the complete genome sequence. *Nature* , 393(6685), 537-44.

¹⁷ Camus JC, Pryor MJ, Médigue C, Cole ST. (2002). Re-annotation of the genome sequence of *Mycobacterium tuberculosis* H37Rv. *Microbiology* . , 148(Pt 10), 2967-73.

¹⁸ <http://www.cbs.dtu.dk/services/TMHMM-2.0/>. (n.d.).

¹⁹ Palmer I, Wingfield PT. (2004). Preparation and Extraction of Insoluble (Inclusion-Body) Proteins from *Escherichia coli*. *Curr Protoc Protein Sci*. (Chapter 6).

²⁰ Clark, E.D.B. (1998). Refolding of recombinant proteins. *Curr. Opin. Biotechnol* , 9, 157-163.

²¹ Middelberg, A.P. (2002). Preparative protein refolding. *Trends Biotechnol* . , 20, 437-443.

²² Annis I, Hargittai B, Barany G. (1997). Disulfide Bond Formation in Peptides. *Methods Enzymo* , 289, 198-221.

²³ Weissman JS, Kim PS. (1992). Kinetic role of nonnative species in the folding of bovine pancreatic trypsin inhibitor. *Proc Natl Acad Sci U S A* . , 89(20), 9900-4.

²⁴ MacDowell, A. A., Celestre, R. S., Howells, M., McKinney, W., Krupnick, J., Cambie, D., Domning, E. E., Duarte, R. M., Kelez, N., Plate, D. W., Cork, C. W., Earnest, T. N., Dickert, J., Meigs, G., Ralston, C., Holton, J. M., Alber, T., Berger, J. M., Agar. (2004). Suite of three protein crystallography beamlines with single superconducting bend magnet as the source. *Journal of synchrotron radiation* , 11, 447-455.

²⁵ Adams, P. D., Afonine, P. V., Bunkoczi, G., Chen, V. B., Davis, I. W., Echols, N., Headd, J. J., Hung, L. W., Kapral, G. J., Grosse-Kunstleve, R. W., McCoy, A. J., Moriarty, N. W., Oeffner, R., Read, R. C., Richardson, J. S., Terwilliger, T. C., and Zwart. (2010). PHENIX: a comprehensive Python-based system for macromolecular structure solution. *Acta Crystallogr D Biol Crystallogr* , 66, 213-221.

²⁶ Pettersen, E. F., Goddard, T. D., Huang, C. C., Couch, G. S., Greenblatt, D. M., Meng, E. C., and Ferrin, T. E. (2004). UCSF Chimera--a visualization system for exploratory research and analysis. *J Comput Chem* , 25, 1605- 1612.

Chapter 3

FtsX-Rv2190c complex.

3.1 Introduction.

Understanding the fundamental mechanism of bacterial cell division is a crucial step toward developing new antibiotics. Cell division is widely studied in *E. coli*¹. The divisome consists of a ring-shaped, multi-protein complex in the center of the cell, where the division process is coordinated and carried out. Many of these proteins have been identified, but some have a redundant role in this process, making the puzzle more complicated to understand. Recently, interactions among three proteins—FtsE-FtsX and EnvC—at the Z ring have been defined². FtsEX is predicted to be a membrane protein complex between an ABC transporter (FtsX) and a cytoplasmic ATP binding cassette (FtsE). EnvC is a protein carrying a predicted coiled-coil domain at the N-terminus and a PG peptidase domain at C-terminus (LytM). The activity of LytM peptidase has not been shown until now, but it has been proven that it interacts and activates AmiA and AmiB, two amidases with PG activity in *E. coli*^{3,4}.

More specifically, interactions have been mapped between the extracellular domain of FtsX and the coiled-coil domain of LytM. The disruption of the interaction is not tolerated by *E. coli* under low osmolarity conditions, while it is tolerated in presence of 0.5% NaCl in culture media. Depletion of one or more of the three genes resulted in long branched cells, completely formed but not separated².

A homologous interaction has been reported in *Streptococcus pneumoniae*, where FtsEX interacts with PcsB⁵, a predicted CHAP peptidase with a similar architecture as LytM: a coiled-coil domain at the N-terminus and a peptidase domain at the C-terminus. Even in *S. pneumoniae*, the deletion of one or more of these three genes generates division defects⁵.

Although *E. coli* and *S. pneumoniae* have different cell shapes and the peptidoglycan assembly processes are slightly different, the interaction between FtsEX and a predicted peptidase is conserved between the two different species. Assuming this

interaction is conserved in other bacteria, this mechanism of regulation becomes of fundamental importance in PG degradation.

In the literature, very little is reported about the FtsE-FtsX system, and most of the studies have been performed in *E. coli*^{6,7,8}. In particular, the role of FtsEX as an ABC transporter in the early or late assembly of the Z ring has been investigated⁹. While the lack of ATP binding to FtsE in the cytoplasm allowed Z ring assembly, it did not allow cells to separate, generating filaments of cells. It appears that the complex is not involved in Z ring assembly, but most likely it seems to be involved with septal ring constriction for divisome proteins. On the other hand, FtsX localizes in absence of FtsE, driving septal constriction of other proteins. These data support the hypothesis that FtsX is more important than FtsE at the septal ring, and ATP hydrolysis might be associated with the propagation through the membrane of a conformational change that stabilizes the dimerization of FtsX^{7,8}. These experimental data seem to exclude the possibility that FtsX could be an ABC transporter, since it is involved in septal constriction.

The latest data on FtsX and peptidases involved in PG hydrolysis raise a very intriguing hypothesis for the role of FtsEX complex. More specifically, the hypothesis is that hydrolysis of ATP in the cytoplasm drives a conformational change in the periplasm that switch hydrolases from an inactive to an active conformation, controlling PG degradation².

In *Mycobacterium tuberculosis*, both FtsE and FtsX are conserved and both are essential proteins¹⁰. Assembly of a *Mtb* FtsEX complex has been shown in *E. coli* cells. The *E. coli* FtsEX has been deleted and substituted by Mt-FtsEX. The *Mtb* complex assembles perfectly well in the different organism and it can completely perform the original function. In addition, the Walker motif for ATP binding in FtsX is completely conserved between *E. coli* and *Mtb*¹¹.

In this chapter, I investigated a possible interaction between FtsX and PG peptidases in *Mtb. Mycobacterium tuberculosis* does not encode a homolog of EnvC, but instead encodes five secreted CHAP like peptidases predicted to be related to PG degradation. Only two, among five peptidases however, encode the predicted coiled coil at the N-terminus that might interact with the extracellular domain of FtsX. We identified an interaction between Rv2190c and FtsX *in vitro*, partially mapped the region of interaction, studied the assembly reaction and determined the stoichiometry of the complex. Our efforts are focused on determining the structure of the FtsX-Rv2190c complex to elucidate the mechanism of interaction and regulation for the two proteins.

3.2 Results.

Mtb encodes 5 NlpC/P60 proteins containing a CHAP-like peptidase domain—Rv0024, Rv1477 (RipA), Rv1478 (RipB), Rv1566c and Rv2190c¹⁰. RipA is the only essential gene of the family, while all the other members might have a certain redundancy. Little is known about the function and the role of all five genes in *Mtb* and in mycobacteria, since all of them are conserved in the genus (Figure 1). Four of these proteins is that they have the catalytic domain at the C-terminus of the sequence, except for Rv1566c, which shows the catalytic domain at the N-terminus. In addition, Rv1566c is predicted to be a non-functioning enzyme, since the catalytic site Cys is replaced by Ala. Only two of the NlpC/P60 proteins have an additional domain of unknown function at the N-terminus. These two proteins are RipA and Rv2190c.

FtsX in *Streptococcus pneumoniae* interacts with the N-terminal domain of a CHAP peptidase⁵. Therefore, to explore the possibility that FtsX shows the same interaction in *Mtb*, we tested the FtsX extracellular domain for interaction with the two long homologs of NlpC/P60 in *Mtb*.

To test the FtsX–RipA and FtsX–Rv2190c interactions, we used two biochemical assays: native gel electrophoresis shift and gel filtration volume shift. Purified RipA and Rv2190c were separated on native gel individually and after incubation with FtsX. Only Rv2190c in presence of FtsX caused a gel shift, indicating an interaction between these two proteins. To the contrary, RipA did not show a shift after incubation with FtsX (Figure2).

In order to confirm the interaction between FtsX with Rv2190c and to investigate the stoichiometry of the complex, we used size exclusion chromatography. The two proteins Rv2190c and FtsX were incubated alone or in combination in a molar excess of FtsX on ice for 30 minute (100 mM NaCl, 20 mM Tris pH 8, 5% glycerol)

and injected for a size exclusion separation. While Rv2190c alone eluted as dimer at 14.68 ml on an analytical S200 column, the mixture of Rv2190c and FtsX co-eluted in a peak at 14.05 ml corresponding to a molecular weight of about 90 kDa, confirming the interaction between the two proteins. An additional small peak at 17.12 ml contained the excess of FtsX used for the reaction (figure 3 and 4).

From the elution data, we can infer that Rv2190c is as a dimer in solution (14.68mL corresponding to a molecular weight of 70 kDa) and FtsX is as a monomer. Once mixed, however, the stoichiometry of the complex becomes 2:2, as shown by the complex elution peak.

To confirm the hypothesis that FtsX interacts only with the N-terminus of Rv2190c, as reported for the *E. coli* and *S. pneumoniae* proteins^{2,5}, we cloned and purified a truncated form of Rv2190c containing only the N-terminus of the protein and tested it for the interaction on the analytical S200 size exclusion column (Figure 5). Even in this case, as for full length Rv2190c, the two proteins co-eluted at 14.64 ml, corresponding to a molecular weight of 70 kDa and confirming also in this case the stoichiometry of the complex as a hetero-tetramer.

Although these data already mapped the interaction of FtsX with the N terminus of Rv2190c, the same experiment was carried out using the C terminus of Rv2190c (data not shown), with negative results. The same approach using size exclusion chromatography was used to confirm the negative preliminary results for RipA and FtsX. We mixed a molar excess of FtsX with RipA for 30 min on ice (100mM NaCl, 20 mM Tris pH 8, 5% glycerol) and injected to an analytical size exclusion column (data not shown). The elution profile showed two different peaks for RipA and FtsX, confirming our preliminary negative results.

3.3 Limited proteolysis of the complex Rv2190c and FtsX.

In order to test the local structural stability of the individual proteins and detect a conformational change due to the formation of the complex between Rv2190c and

FtsX, we performed limited proteolysis with different proteases. A concentration of 1mg/ml of Rv2190c, FtsX and complex Rv2190c-FtsX were mixed with trypsin at 1000:1, and the degradation reactions were followed using time points from 0 to 4 hours. Limited proteolysis time course results showed a different profile for Rv2190c alone compared to the complex with FtsX (Figure 6). More specifically after four hours, Rv2190c was completely degraded and the denaturing gel showed a main stable band at 25 kDa. Rv2190c in presence of FtsX showed instead a doublet of 2 bands around 18 kDa and the original FtsX band at 15 kDa, which was stabilized in the presence of protease.

Limited proteolysis using trypsin in a 500:1 ratio gave the same results, confirming two different stable cores for Rv2190c and Rv2190c-FtsX (Figure 6). These data suggest conformational changes for Rv2190c in complex with FtsX. In contrast, the FtsX is equally stable over time in the presence and absence of Rv2190c. After that, we studied the proteolysis time course reaction for FtsX, using trypsin and thermolysin in a 5:1 ratio of protein:protease (Figure 7). A Coomassie-stained gel bands showed two different profiles of degradation for FtsX. The different profiles were due to the two different proteases used and some uncleaved FtsX, even after 4 hours of incubation with high ratio of protease. These results confirm that FtsX probably has a stable protein core that is completely folded.

We cut out gel bands corresponding to proteolysis products at 4 hours, further digested with trypsin, and analyzed peptides by LC-MS/MS. We used the collection of peptides detected by mass spectrometry to infer the conformational changes in Rv2190c in the presence of FtsX and, more importantly, to map the domains of interaction of the two proteins (Table 1).

Rv2190c was subjected to protease cleavages at the N terminus, (peptides mapped to the sequence from 100 to the end). In contrast, Rv2190c in complex with FtsX showed a different profile, with the greatest protection of amino acids 10-180. Our limited proteolysis results show that Rv2190c interacts with FtsX at the N-terminus,

making the C-terminus of the protein sensitive to protease cleavages. To the contrary, Rv2190c alone is well packed at the C-terminus and the N-terminus is sensitive to proteolysis.

3.4 Rv2190c crystallization.

Rv2190c N-terminus, Rv2190c C-terminus, full-length Rv2190c, FtsX and the Rv2190c-FtsX complex were tested for crystallization by hanging drop vapor diffusion. About 1000 different conditions were tested for each protein and for the complex. The Rv2190c C-terminus at concentrations between 12 mg/mL and 24 mg/mL failed to crystallize. The Rv2190c N-terminus that was not stable at room temperature during the purification was set up for crystallization at 4 °C, but failed to crystallize as well. Rv2190c at a concentration of 12 mg/mL set up for crystallization at 18 °C showed rapid, heavy, irreversible precipitation with no possibility of crystallization. The latest results are unusual, because the crystallization drops did not show uniform precipitation, suggesting intrinsic protein instability in solution and/or polydispersity. To test the status of the protein in solution and to investigate a possible condition where Rv2190c is monodisperse, we incubated the protein overnight in 24 different conditions plus or minus 100 mM salt and 5% glycerol for a range of pH starting from 3.5 up to 10. All the drops were analyzed by dynamic light scattering (DLS)¹². None of the 48 conditions analyzed produced monodisperse Rv2190c. Due to the negative DLS results and heavy precipitate in the crystallization drops, we hypothesized that Rv2190c might have a mobile domain interchanging between different conformations.

3.5 Rv2190c-FtsX crystallization.

We mixed a purified Rv2190c with an excess of FtsX for a further separation on the analytical size exclusion S200. Pooling only the fractions where both proteins

showed a 1:1 ratio on SDS polyacrylamide gel electrophoresis (PAGE), we concentrated the complex to 10mg/mL, and tested for crystallization in almost 500 conditions. After 8 hours almost 50% of the conditions showed a precipitate and 8 conditions showed crystals. All the conditions generating crystals were around pH 8 and all contained PEG 8000 at different concentrations. The crystals were easily reproducible.

The best crystals were harvested, frozen in liquid nitrogen, and diffraction images were collected at beamline 8.3.1 at the Advanced Light Source¹³. The crystals diffracted poorly, giving reflections to only 20-30 Å resolution. This diffraction pattern is typical of big unit cells, containing a lot of solvent. To improve the diffraction pattern, we tried to dehydrate crystals to reduce the unit cell dimensions and improve packing. This procedure was unsuccessful^{14,15}. Next we tried to treat the complex with a protease directly in the crystallization drop to remove a possible flexible domain. This procedure improved the resolution of the diffraction pattern to 8 Å. ThisWe tested also for crystallization the complex of the N terminus of Rv2190c and FtsX, but no crystals were observed.

3.6 Discussion.

The activation of PG hydrolysis is highly regulated to reduce toxicity in bacteria. It has been shown in *E. coli* and *S. pneumonia* that ATP hydrolysis in the cytoplasm is directly related to the hydrolysis of peptidoglycan in the periplasm^{2,5}. This mechanism has been investigated for the FtsEX complex, EnvC and PcsB, respectively, in *E. coli* and *S. pneumonia*^{2,5}.

Here, we report an analogous interaction in mycobacteria. *Mycobacterium tuberculosis* encodes two NlpC/P60 proteins containing a large N-terminal domain, predicted to form a coiled coil. One of these two proteins, RipA, is essential, but the other one, Rv2190c, is not. Recently, the role of Rv2190c has been investigated for cell growth and infection¹⁶. Even if Rv2190c is not an essential protein in *Mtb*, the lack of this gene reduced cell-wall integrity. The defects showed by the *Rv2190c M. tuberculosis* mutant were not related to septation, but to cell wall integrity. The cells exhibited altered PDIM secretion and an increased susceptibility to lysozymes¹⁷. During infection, the lack of Rv2190c caused attenuated growth in the lung but not in the spleen. The insertion of the only catalytic domain of Rv2190c did not support normal growth. These results highlight that the missing part of the protein (the N-terminus) might play a key role in regulation. Moreover, this study shows Rv2190c is expressed during cell growth *in vitro* and during infection *in vivo*, and the lack of this gene weakens cell-wall integrity. A different study in *C. glutamicum* and *Mtb* showed FtsEX was involved in cell wall defects under ethambutol stress¹⁸.

In literature, the role of FtsEX as ABC transporter is controversial. Based on the amino acid sequence, it is unlikely that FtsX can be an ABC transporter where the ATP hydrolysis controls the transport across the membrane. Usually ABC transporters encode 7 or 8 trans-membrane helices and the process of dimerization allows the formation of large channels able to transport large molecules across the membrane. In the case of FtsX, it would be only a small ABC transporter since it encodes only 4 trans-membrane domains and a large extracellular domain, with the

consequent impossibility to transport large molecules. Moreover, the lack of any charged amino-acids in the sequence of trans-membrane helixes restricts the range of molecules that can be transported to only hydrophobic molecules.

FtsX in Mycobacteria encodes an additional motif conserved only in mycobacteria and corynebacteria (G+C rich bacteria) in the large extracellular domain with two Cys distant one from the other only five amino acids CXXXXC. We investigated by biochemical methods whether or not Cys might coordinate a metal like zinc or be involved in intra or intermolecular disulphide bridges, with negative results. The role of the two Cys is still unknown and very intriguing since it is conserved only in GC rich bacteria¹⁹.

In this work we proved the same interaction *in vitro* for *Mtb* similar to what has been already observed for *E. coli* and *S. pneumoniae*. We show FtsX interacts with Rv2190c but not with RipA probably because the two proteins are related to different pathways in the synthesis and degradation of peptidoglycan in mycobacteria.

Our studies *in vitro* explored the mechanism of assembling for the complex and we established the stoichiometry of the membrane complex. We proved with biochemical method that Rv2190c is a dimer in solution and that monomeric FtsX dimerizes in presence of Rv2190c. The stoichiometry ratio is very important to understand how the complex works. The hypothesis proposed in the published work was that ATP binds to FtsE and the hydrolysis might allow FtsX dimerization or communicate a conformational change to the periplasm. Our results exclude the possibility ATP plays a role in FtsX dimerization. Also, based on our limited proteolysis results, we can state the interaction between FtsX and Rv2190c is already enough to establish conformational change on Rv2190c, even though we haven't investigated yet the capability of Rv2190c-FtsX to hydrolyse PG.

More specifically Rv2190c C terminus is resistant to proteases cleavages, probably due to a very well packed catalytic domain, instead the FtsX complex stabilizes and protects the N terminus of Rv2190c making its catalytic domain completely exposed. Our results go towards the assumption that the dimerization condition of Rv2190c in solution is the way to keep the catalytic domain in an inactive state. We

have already seen how RipA²¹ and RipB block the access of substrate to the catalytic site with the auto-inhibited folding. Under the interaction with FtsX a big conformational change is observed by limited proteolysis since the protected folding region is completely inverted.

Taken together, limited proteolysis data and complex assembling, might have a role on the activation of Rv2190c due the conformational changes.

Therefore, our results exclude the possibility ATP plays a role in FtsX dimerization and propagation of conformational changes through the membrane. Within the hypothesis formulated until now, regarding FtsEX complex, our results leave open the possibility that the hydrolysis of ATP might help FtsEX stabilization or proteins constriction at the septum.

It can be also possible that ATP hydrolysis might stress the conformational changes we already observed for Rv2190c. However, we cannot exclude a possible role of ATP in Rv2190c catalytic activation, since we have not tested yet Rv2190c – FtsX complex activity on PG.

In conclusion, our data are very critical to elucidate the mechanism of interaction *in vitro* between FtsX and Rv2190c. Both proteins are related to cell wall integrity and osmotic stress in *Mtb*, and probably constitute a fundamental pathway highly conserved. Solving the structure of the complex or even only of FtsX can be of crucial importance to understand function and role of these proteins.

3.7 Materials and Methods.

FtsX extracellular domain cloning expression and purification.

Oligonucleotide primers were designed to amplify nucleotide sequence corresponding to the Rv3101c extracellular domain by PCR using H37Rv genomic DNA. Primer sequences contained the insertion site for the TOPO TEV vector. The PCR product was cloned in an expression vector (pHMGWA Gateway) carrying a TEV cleavable N-terminal HisMBP tag. The positive plasmid was transformed into the Rosetta2(DE3)pLysS expression system.

Cells were grown at 37 °C until OD 0.6 was reached, then cultures were induced with 1mM IPTG at 18 °C and left overnight for protein expression. The pellet was resuspended in Buffer A (300 mM NaCl, 20 mM Tris pH 8, 20 mM imidazole, 10% glycerol, 0.5 mM TCEP) containing protease inhibitors. The pellet was sonicated and the lysate was centrifuged at 18000 rpm for 1 hour. FtsX–HisMBP was separated by affinity chromatography a Ni-affinity column. The column was washed with 10 volumes of Buffer A. The protein was eluted with Buffer B (300 mM NaCl, 20 mM Tris pH 8, 0.5 mM TCEP, 300 mM imidazole, 10% glycerol). TEV protease was added, and the protein was dialyzed against buffer A overnight to remove excess imidazole. The product of TEV cleavage was further purified by an additional affinity chromatography step using a Ni-affinity column to remove the HisMBP and TEV protease. The flow-through containing the protein of interest was concentrated and injected for a further purification step by size exclusion chromatography. The elution profile showed a large peak corresponding to molecular weight 15 kDa. The protein was flash frozen in liquid nitrogen and stored at -80 °C for further experiments.

Native gel shift.

Protein binding reactions were carried out 100mM NaCl, 20 mM Tris pH 8, 5% glycerol. Equimolar amounts of Rv1477 and Rv2190c were incubated in presence or absence of FtsX for 45min on ice. Reactions were separated by native gel

electrophoresis in native gel buffer (0.025 M Tris, 0.192 M glycine, pH 8.5) at 4 °C (60V) for 3 hours using the BioRad 4-20% Tris-Glycine gel system. Gel shifts were analyzed by Coomassie blue stain.

Limited proteolysis.

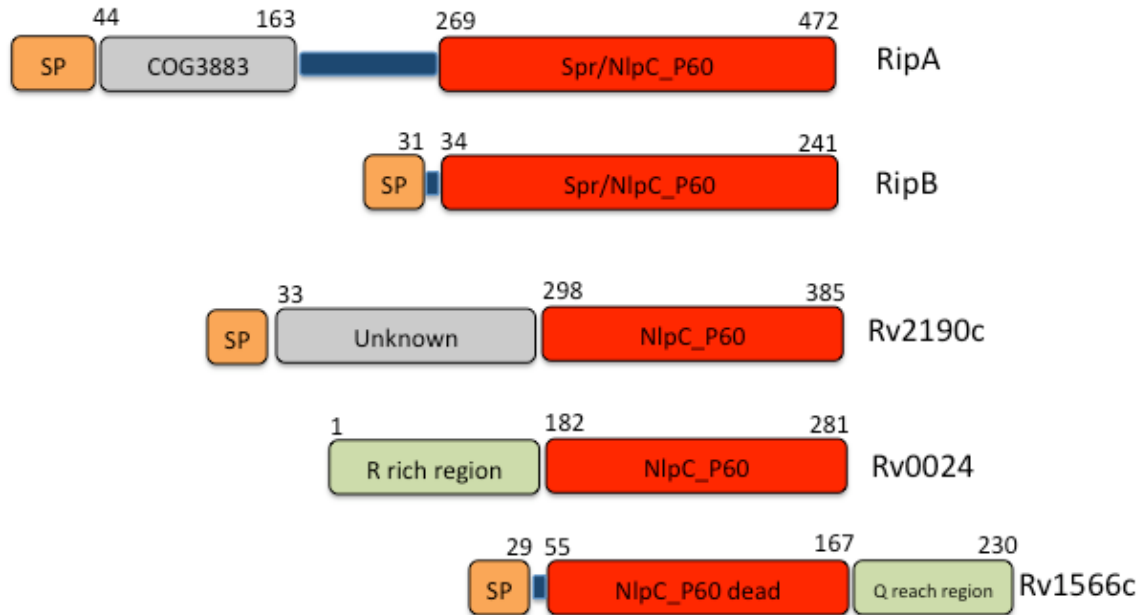
Limited proteolysis reactions were carried out in 150 mM NaCl, 20 mM Tris pH 8.0, 5% glycerol. For binding reactions, Rv2190c and FtsX were first mixed at equimolar ratio for 15 minutes at room temperature. FtsX, Rv2190c and Rv2190c-FtsX complex were mixed with trypsin at a mass ratio of 1:1000 and 1:500 at 4 °C. A volume of 10 µL for each time point corresponding to input, 0 min, 5 min, 10 min, 30 min, 1 hour, 2 hours and 4 hours were stopped adding 1 µL of 1% TFA and 5 µL SDS-PAGE loading buffer. Protein fragments were separated by gel electrophoresis using the BioRad 4-20% Tris-Glycine gel system and stained by Coomassie blue. Two additional limited proteolysis reactions were carried out for FtsX alone using trypsin and thermolysin at a mass ratio of 1:10.

Crystallization.

The Rv2190c-FtsX complex purified by size exclusion chromatography and concentrated to 10 mg/mL was screened for crystallization using 5x96 commercially available conditions in a 1:1 protein:reservoir ratio. After 8 hours crystals appeared in 8 different conditions. The best crystals grew in 0.2 M NaCl, Tris pH 7.8 and 20% PEG 8000. The drop was scaled up and the crystals were easily reproduced. The same kind of crystal was optimized for better diffraction. Dehydration was carried out in the same crystallization condition using 25% and 30% PEG 8000. Crystals were also optimized using proteases in the crystallization drop. At a mass ratio of 1:10000 and 1:20000, trypsin and chymotrypsin were mixed in a volume 1:0.5:0.5 µL protein:reservoir:protease solution to allow a better crystal packing.

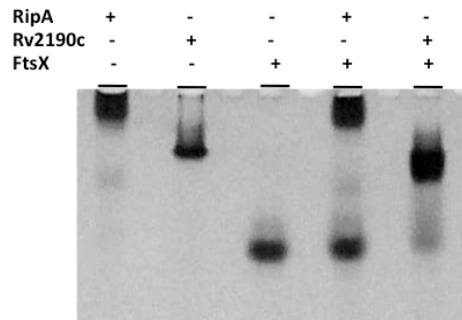
3.8 Figures.

Figure 1. NLPC/P60 family in *Mycobacterium tuberculosis*.



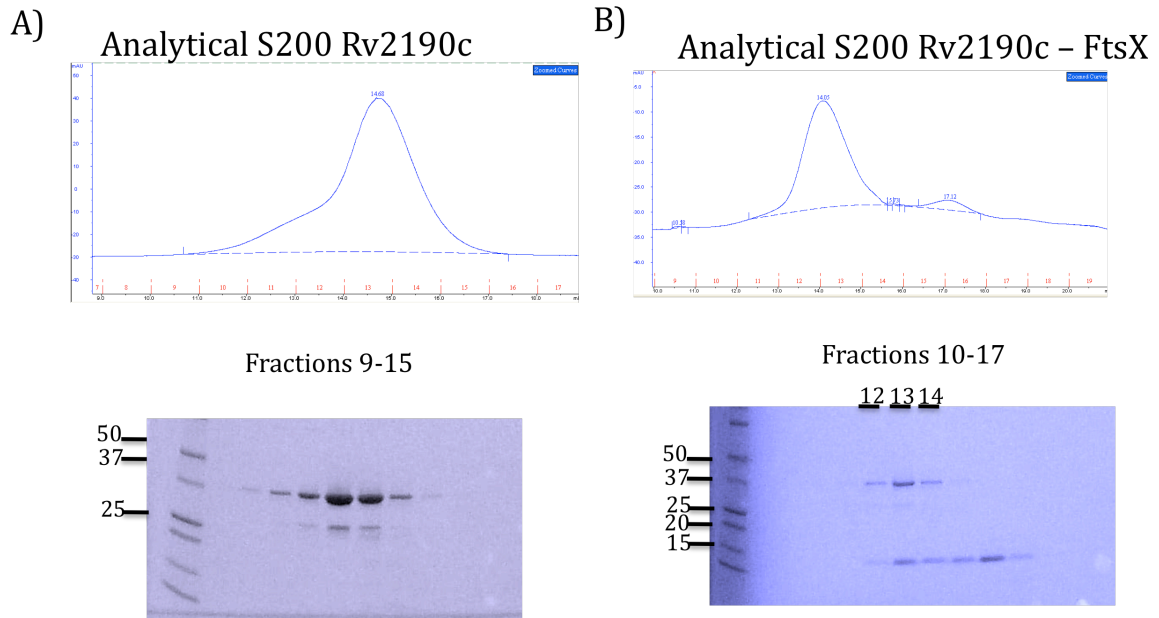
Schematic view of all five NlpC/P60 proteins in *Mtb* showing the domains encoded in these proteins.

Figure 2. Native gel for FtsX, RipA, and Rv2190c.



Native gel showing a migration shift for Rv2190c and FtsX bands. The same shift is not observed For RipA and FtsX, excluding any possible interaction between them.

Figure 3. Analytical size exclusion chromatography for Rv2190c and Rv2190c-FtsX complex.



A) Analytical size exclusion chromatography for Rv2190c. Rv2190c elutes at 14.68 ml and it is a dimer in solution. B) Analytical size exclusion chromatography for Rv2190c - FtsX. The complex elutes at 14.05 ml as a dimer of dimers.

Figure 4. Analytical size exclusion for FtsX.

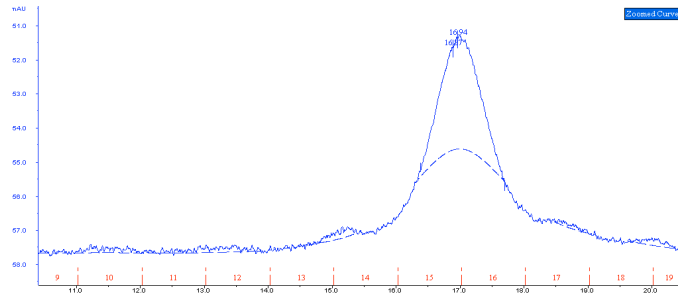
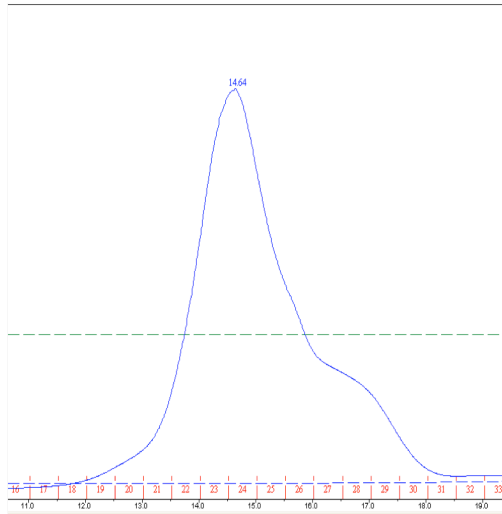


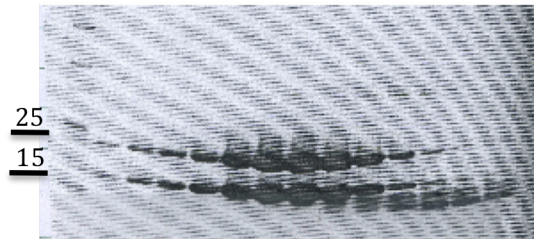
Figure 4. Analytical size exclusion for FtsX. FtsX is a monomer in solution and elutes at a volume of 17.0 ml.

Figure 5. Analytical size exclusion chromatography for FtsX and Rv2190c N-terminus.

Analytical S200

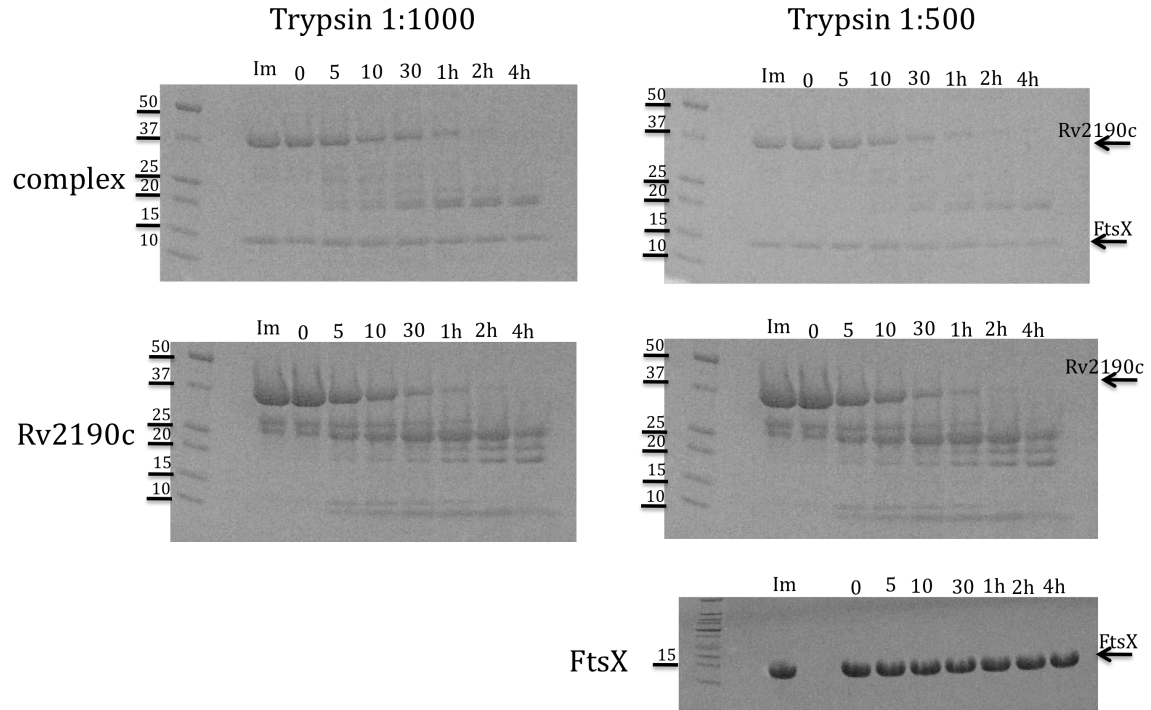


Fractions 18-30



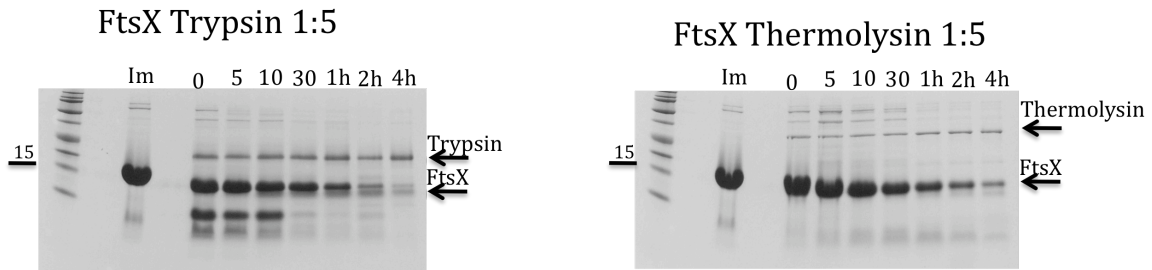
The complex runs at an apparent molecular weight of 70 kDa (14.74 ml) as a hetero-tetramer. Coomassie stained gel shows an equimolar ratio for both protein bands.

Figure 6. Limited proteolysis for Rv2190c, FtsX, and Rv2190c-FtsX complex.



Limited proteolysis using a mass ratio of 1:1000 and 1:500. Rv2190c alone and Rv2190c-FtsX complex show different profiles of proteolysis. FtsX alone is very stable to proteolysis.

Figure 7. Limited proteolysis on FtsX using a large amount of protease.



Even when using a large amount of protease, FtsX is a highly resistant to degradation.

3.9 Tables.

Table 1. MS/MS results on limited proteolysis bands for Rv2190c and Rv2190-FtsX complex.

<u>10</u>	<u>20</u>	<u>30</u>	<u>40</u>	<u>50</u>	<u>60</u>	
DPADDALAKL	NELSRQAEQT	TEALHSAQLD	LNEKLAAQRA	ADQKLADNRT	ALDAARARLA	
	<u>70</u>	<u>80</u>	<u>90</u>	<u>100</u>	<u>110</u>	<u>120</u>
TFQTAVNKVA	AATYMGGRTH	GMDAILTAES	POLLIDRLSV	QRVMAHQMST	QMARFKAA3GE	
	130	140	150	160	170	180
<u>QAVKAEQAAA</u>	<u>KSAADARSAA</u>	<u>EQAAAVRANL</u>	<u>QHKQSLOLQVQ</u>	<u>IAVVKSQYVA</u>	<u>LTPEERTALA</u>	
	190	200	210	220	230	240
<u>DPGPVPAVAA</u>	<u>IAPGAPPAAL</u>	<u>PPGAPPGDGP</u>	<u>APGVAPPPGG</u>	<u>MPGLPFVQPD</u>	<u>GAGGDRTAVV</u>	
	250	260	270	280	290	300
<u>QAALTOVGAP</u>	<u>YAWGGAAPGG</u>	<u>FD</u> C <u>SGLVMWA</u>	<u>FOQAGIALPH</u>	<u>SSQALAHGGO</u>	<u>PVALSDLQPG</u>	
	310	320	330	340		
<u>DVLTFYSDAS</u>	<u>HAGIYIGDGL</u>	<u>MVHSSTYGVP</u>	<u>VRVVPMDSSG</u>	<u>PIYDARRY</u>		

Rv2190c amino acid sequence. The blue sequences represent the peptides detected by LC-MS/MS for the Rv2190c-FtsX complex. The underlined sequence represents peptides detected by LC-MS/MS for Rv2190c alone. In red is highlighted the catalytic Cys.

3.10 References.

- ¹ de Boer PA. (2010). Advances in understanding E. coli cell fission. *Curr Opin Microbiol. , Dec;13(6)*, 730-7.
- ² Yang DC, Peters NT, Parzych KR, Uehara T, Markovski M, Bernhardt TG. (2011). An ATP-binding cassette transporter-like complex governs cell-wall hydrolysis at the bacterial cytokinetic ring. *Proc Natl Acad Sci U S A. , Nov 8;108(45):*, 1052-60.
- ³ Peters NT, Dinh T, Bernhardt TG. (2011). A fail-safe mechanism in the septal ring assembly pathway generated by the sequential recruitment of cell separation amidases and their activators. *J Bacteriol. , Sep;193(18):*, 4973-83.
- ⁴ Uehara T, Parzych KR, Dinh T, Bernhardt TG. (2010). Daughter cell separation is controlled by cytokinetic ring-activated cell wall hydrolysis. *EMBO J. , Apr 21;29(8)*, 1412-22.
- ⁵ Sham LT, Barendt SM, Kopecky KE, Winkler ME. (2011). Essential PcsB putative peptidoglycan hydrolase interacts with the essential FtsXSpn cell division protein in *Streptococcus pneumoniae* D39. *Proc Natl Acad Sci U S A. , Nov 8;108(45)*, 1061-9.
- ⁶ de Leeuw E, Graham B, Phillips GJ, ten Hagen-Jongman CM, Oudega B, Luirink J. (1999). Molecular characterization of *Escherichia coli* FtsE and FtsX. *Mol Microbiol. , Feb;31(3)*, 983-93.
- ⁷ Schmidt KL, Peterson ND, Kustusich RJ, Wissel MC, Graham B, Phillips GJ, Weiss DS. (2004). A predicted ABC transporter, FtsEX, is needed for cell division in *Escherichia coli*. *J Bacteriol. , Feb;186(3)*, 785-93.
- ⁸ Arends SJ, Kustusich RJ, Weiss DS. (2009). ATP-binding site lesions in FtsE impair cell division. *J Bacteriol. , Jun;191(12)*, 3772-84. Corbin BD, Wang Y, Beuria TK, Margolin W. (2007).
- ⁹ Corbin BD, Wang Y, Beuria TK, Margolin W. (2007). Interaction between cell division proteins FtsE and FtsZ. *J Bacteriol. , Apr;189(8)*, 3026-35.
- ¹⁰ Cole ST, Brosch R, Parkhill J, Garnier T, Churcher C, Harris D, Gordon SV, Eiglmeier K, Gas S, Barry CE 3rd, Tekaia F, Badcock K, Basham D, Brown D, Chillingworth T, Connor R, Davies R, Devlin K, Feltwell T, Gentles S, Hamlin N, Holroyd S, Hornsby T, Jage. (1998). Deciphering the biology of *Mycobacterium tuberculosis* from the complete genome sequence. *Nature , 393(6685)*, 537-44.
- ¹¹ Mir MA, Rajeswari HS, Veeraraghavan U, Ajitkumar P. (2006). Molecular characterisation of ABC transporter type FtsE and FtsX proteins of *Mycobacterium tuberculosis*. *Arch Microbiol. , Mar;185(2)*, 147-58.
- ¹² Jancarik J, Pufan R, Hong C, Kim SH, Kim R. Source . (2004). Optimum solubility (OS) screening: an efficient method to optimize buffer conditions for homogeneity and crystallization of proteins. *Acta Crystallogr D Biol Crystallogr. , Sep;60(Pt 9)*, 1670-3.
- ¹³ MacDowell, A. A., Celestre, R. S., Howells, M., McKinney, W., Krupnick, J., Cambie, D., Domning, E. E., Duarte, R. M., Kelez, N., Plate, D. W., Cork, C. W., Earnest, T. N., Dickert, J., Meigs, G., Ralston, C., Holton, J. M., Alber, T., Berger, J. M., Agar. (2004). Suite of three protein crystallography beamlines with single superconducting bend magnet as the source. *Journal of synchrotron radiation , 11*, 447-455.

-
- ¹⁴ Heras B, Edeling MA, Byriell KA, Jones A, Raina S, Martin JL. (2003). Dehydration converts DsbG crystal diffraction from low to high resolution. *Structure*. , Feb;11(2), 139-45.
- ¹⁵ Heras B, Martin JL. (2005). Post-crystallization treatments for improving diffraction quality of protein crystals. *Acta Crystallogr D Biol Crystallogr*. , Sep;61(Pt 9), 1173-80.
- ¹⁶ Parthasarathy G, Lun S, Guo H, Ammerman NC, Geiman DE, Bishai WR. (2012). Rv2190c, an NlpC/P60 Family Protein, Is Required for Full Virulence of *Mycobacterium tuberculosis*. *PLoS One*. , 7(8), e43429.
- ¹⁷ Cox JS, Chen B, McNeil M, Jacobs WR Jr. (1999). Complex lipid determines tissue-specific replication of *Mycobacterium tuberculosis* in mice. *Nature*. , Nov 4;402(6757), 79-83.
- ¹⁸ Radmacher E, Stansen KC, Besra GS, Alderwick LJ, Maughan WN, Hollweg G, Sahm H, Wendisch VF, Eggeling L. Source . (2005). Ethambutol, a cell wall inhibitor of *Mycobacterium tuberculosis*, elicits L-glutamate efflux of *Corynebacterium glutamicum*. *Microbiology*. , May;151(Pt 5), 1359-68.
- ¹⁹ Brenner S.E. (1998). Practical database searching. *Trends in Biotechnology* , 16, 9-12.
- ²¹ Ruggiero A, Marasco D, Squeglia F, Soldini S, Pedone E, Pedone C, Berisio R. (2010). Structure and functional regulation of RipA, a mycobacterial enzyme essential for daughter cell separation. *Structure* , 18(9), 1184-90.

Chapter 4

RpfE crystal structure reveals a positively charged catalytic cleft.

4.1 Introduction.

Before the discovery of resuscitation promoting factor (Rpf) proteins, the mechanism by which bacteria are able to switch from dormancy to vegetative growth was unknown. Many pathogens, including *Mycobacterium tuberculosis*, can enter in a reversible dormant state with a low metabolic activity for an extended period of time until the environmental condition changes to favor growth. In 1998, Rpf proteins were discovered in *Mycrococcus luteus* and associated to the ability of bacteria to exit from dormancy^{1,2}. Indeed Rpf proteins added to dormant cultures were able to stimulate growth. Their activity is related to degradation of the bacterial cell wall³.

Mycobacterium tuberculosis encodes five resuscitation promoting factor proteins, RpfA-E. In *Mtb*, no member of this family is an essential protein. Deletion of each single gene did not produce any differences in the mycobacterial cells, leading to the suggestion of redundancy among these proteins. However, combined deletions of at least three Rpf genes exhibited growth defects *in vitro*, showing a discrete function of Rpf proteins in *Mtb*. Moreover, the *RpfB* deletion mutant failed to resuscitate in mice, while RpfE was found to play an important role in switching mycobacterial cultures from slow to fast growth. These results rank RpfB and RpfE as the most important Rpf proteins^{4,5,6,7}.

Even though none of these proteins seems essential for growth *in vitro*, RpfB performs a very important function in infection. The Rpf family is thought to promote resuscitation of dormant cells by hydrolyzing peptidoglycan to release an active fragment. This fragment signals to the extracellular domain of PknB, which signals the transition from dormancy to vegetative growth^{8,9}. In *Mtb*, Rubin and coworkers^{10,11} reported the interaction between RpfB-E and RipA, a peptidase that cleaves the bond between D-Ala-DAP in peptidoglycan. The fragments released by RpfE-B and RipA cleavage are most likely the candidate signals for cell reactivation.

RpfE is a secreted protein that encodes only the catalytic domain and a low complexity region at the N terminus. In this chapter, we describe the investigation performed for the interaction between RpfE and RipA *in vitro*, with the same approaches we used to test for the interaction between RipA and RpfB. We solved the structure of RpfE at 2.76-Å resolution after spending a long time troubleshooting the crystallization. The structure showed that RpfE and RpfB differ in the charge of the active site, with RpfE containing many more basic residues that likely contribute to the specificity of substrate recognition.

4.2 RpfE and RipA interaction.

Given our negative results for the interaction between RipA and RpfB, we pursued our goal to activate RipA by protein-protein interaction. Rubin and coworkers reported not only the interaction of RipA with RpfB, but also with RpfE. Both RpfB and RpfE were reported to interact with the C-terminus of RipA. Using the yeast two-hybrid method, the interaction was mapped to the last 20 amino acids of RipA .

To reconstitute this interaction *in vitro*, we cloned the RipA₂₆₃₋₄₇₂ C-terminal catalytic domain (the same truncation we used to test for the interaction with RpfB) in a polycistronic plasmid 2E with RipA carrying a strep tag and a combination of 4 different tags for RpfE (His-MBP, His-Sumo, HisTrx, His-mOCR). All 4 polycistronic plasmids carrying truncations of RipA and RpfE did not produce any colonies, even after two days of incubation at 37 °C. We don't know the reason that colonies did not grow, but these plasmids clearly carried combinations of genes that are toxic for *E. coli*.

To produce the proteins for interaction studies, we expressed and purified RipA and RpfE separately. We tested the interaction by native electrophoresis gel shift (data not shown) and by size exclusion chromatography. A molar excess of RipA was mixed with RpfE and incubated on ice for 30 min. The elution chromatogram of the size exclusion column showed two separated peaks with negative results for interaction (Figure 1).

4.3 RpfE structure.

To characterize RpfE, we expressed the catalytic domain using a HisMBP-tag fusion in *Escherichia coli*. Based on a sequence alignment of mycobacterial resuscitation promoting factors, RpfE conserves the two Cys residues that form a disulphide bond in RpfB. Thus, RpfE likely conserves the disulphide bond. To produce the disulphide

bond, we added a step to the purification to oxidize the two Cys using a mixture of 10:1 of reduced to oxidized glutathione¹².

Once purified (in 0.1M NaCl, 20 mM Tris pH 8, 5% glycerol), the protein crystallized in almost 80% of more than 500 conditions screened. The crystals grew as tiny needles. To improve the RpfE crystals, we changed the amount of salt¹³ in the protein buffer from 0.1 M NaCl to 0.3 M NaCl. This change decreased sharply the number of conditions with crystals, but the crystals were still small. Different pHs for crystallization were also tested without any improvement¹⁴. We harvested the best looking and biggest needles and found one crystal that diffracted to 2.76-Å resolution in a condition containing PEG 3350 and a mixture of small molecules at pH 6.5.

The structure was determined using molecular replacement with RpfB as a search model. Six RpfE molecules were packed in the asymmetric unit (Figure 2). The protein fold contains 6 alpha helices connected by loops of various lengths and a disulphide bond between Cys 107 and Cys 168 (Figure 3).

Overall RpfE conserves the predicted catalytic glutamate (Glu108) and the catalytic cleft typical of lysozymes. As reported for the RpfB structure¹⁵ (PDB ID 3E05), the Asp involved in lysozyme catalysis is replaced by a Tyr (Figure 3). The lack of the Asp in the catalytic cleft is probably responsible of different mechanism of cleavage of the beta-1,4-glycosidic bond, classifying the enzyme as a lytic transglycosylase.

4.4 Comparison between RpfB and RpfE.

Based on Blast alignments among resuscitation promoting factors in *Mtb*, we observed high conservation in the catalytic domain, with 67% sequence identity between RpfE, RpfB, and RpfC; 64% sequence identity between RpfE and RpfA, and 61% between RpfE and rpfD¹⁶. Even though RpfB and RpfE show 67% sequence

identity and the two structures superimpose closely, the RpfE sequence contains many more Arg residues. This difference in the amino-acid sequence composition makes the RpfE catalytic domain a basic protein, compared to the RpfB catalytic domain that instead shows a pI around 5.5. This difference between the two proteins does not cause large differences in structure (Figure 4), but instead reveals a dramatic difference in the charge state of protein surface on the side accommodating the catalytic cleft (Figure 5). While RpfB presents negatively charged surface patches around the catalytic cleft, RpfE instead shows a positively charged catalytic cleft. The charge differences also occur on the surface surrounding the cleft.

4.5 Discussion.

The unique role of each Rpf protein has not been fully elucidated yet. Among the five Rpf proteins in *Mtb*, the transglycosylase domain is highly conserved, but the additional domains are predicted to have different functions. RpfB, for example, encodes a domain of unknown function and a G5 domain probably involved in N-acetyl-glucosamine recognition. RpfE and RpfA encode long Pro-rich regions at the N-terminus and the C-terminus, respectively¹⁷. Even though Rpf functions may have a certain redundancy, they also have distinct roles in resuscitating mycobacterial cells in infected mice and in mycobacterial growth *in vitro*¹⁸.

Nevertheless, the RpfE crystal structure is very similar to the catalytic domain of RpfB. The structures, however, reveal a dramatic difference in charges on the surface of catalytic cleft. The RpfE catalytic cleft is basic at neutral pH, while the cleft of RpfB is acidic. The different charge states in the catalytic cleft denote differences in substrate binding and the pH optima of catalysis. Glycan strands in peptidoglycan are conserved among bacteria. In mycobacteria, however, the NAM is sometimes modified with a N-glycolyl instead of N-acetyl¹⁹. The positively charged pocket of RpfE might better accommodate the hydroxyl group. We cannot exclude also that RpfE binds glycan strands with a different saccharide stereochemistry or show a different pH dependence of hydrolysis. The charge differences extend to the surface of the side that accommodates the catalytic cleft, supporting the idea that they interact with different PG structures.

The RpfE structure shows how a few changes in the amino-acid sequence can become a crucial difference for substrate binding, catalytic activity or potential protein-protein interactions. Our structure reveals the first evidence that these two enzymes may act on different substrates. The Rpf family has a role in resuscitating dormant mycobacteria by releasing a fragment of peptidoglycan, which signals the reactivation of metabolism. The difference in the fragment released might

discriminate between pathways of resuscitation or signal an improvement in the rate of growth⁷.

4.6 Material and Methods.

RpfE (Rv2450c) cloning, expression, purification, crystallization and structure determination. Oligonucleotide primers were designed to amplify nucleotide sequence corresponding to the RpfE catalytic domain by PCR using H37Rv genomic DNA. Primer sequences contain the insertion for TEV cleavage. The PCR product was cloned in an expression vector (2MT vector <http://www.addgene.org>.) carrying a TEV protease cleavage site and N-terminal HisMBP tag. The positive plasmid was transformed into the Rosetta2(DE3)pLysS expression system.

Cells were grown at 37 °C until OD₆₀₀ 0.6 was reached, and cultures were induced with 1mM IPTG at 16 °C and shaken overnight for protein expression. The pellet was resuspended in Buffer A (300 mM NaCl, 20 mM imidazole, 20 mM Tris pH 8, 10% glycerol, 0.5 mM TCEP), containing protease inhibitor cocktails. The pellet was sonicated and the lysate centrifuged at 18000 rpm for 1 hour. Supernatant was loaded onto a Ni-affinity column and washed with 10 volumes of Buffer A. Protein was eluted with Buffer B (300 mM NaCl, 20 mM Tris pH 8, 0.5 mM TCEP, 300 mM imidazole). TEV protease was added, and the protein was dialyzed against buffer A overnight to remove the excess of imidazole. In the same dialysis buffer, a 1:10 ratio of reduced glutathione *versus* oxidized glutathione was added to promote Cys oxidation to disulphide bonds.

The reaction mixture was purified using an additional affinity chromatography step on a Ni column to remove the tag and TEV protease. The flow through was concentrated and further purified on a preparative Superdex S75 size exclusion column. Elution fractions were collected and investigated by Coomassie blue-stained SDS PAGE. The fractions containing RpfE were concentrated to 12mg/ml, and the protein was screened for crystallization by hanging drop vapor diffusion.

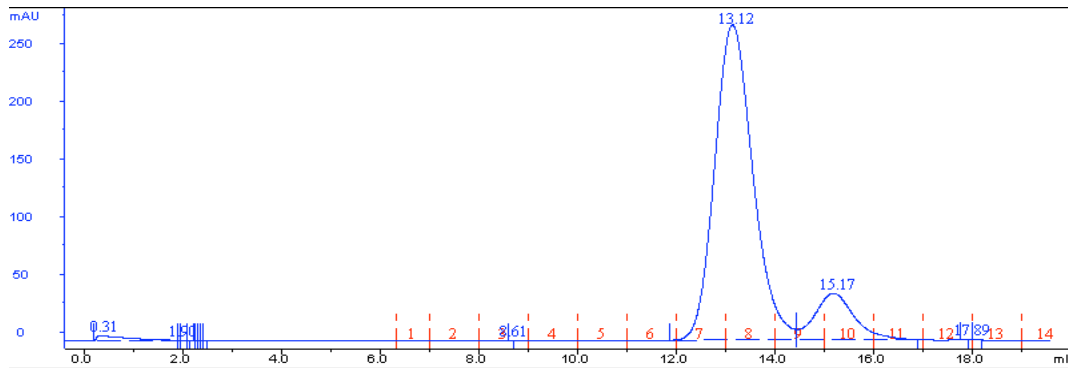
Many different crystals generated in different conditions were screened for diffraction. Diffraction data were collected at the Lawrence Berkeley National

Laboratory Advanced Light Source Beamline 8.3.1²⁰. The PHENIX²¹ software suite was used for model building by molecular replacement using the RpfB homolog (3E05 in Protein Data Bank (PDB)) as the search model. Cycles of refinement were performed by with PHENIX. Images and structural alignments were generated using Chimera software²².

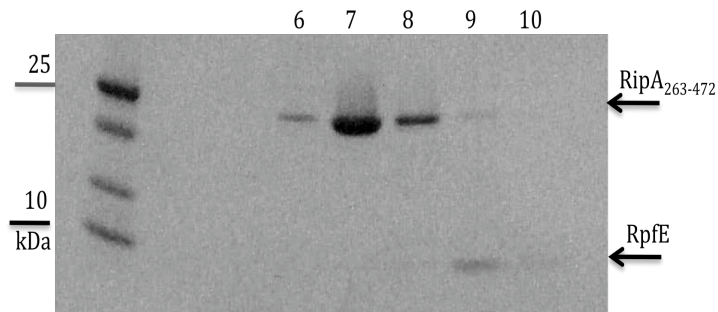
4.7 Figures

Figure 1. Analytical size exclusion of RpfE and RipA.

A)

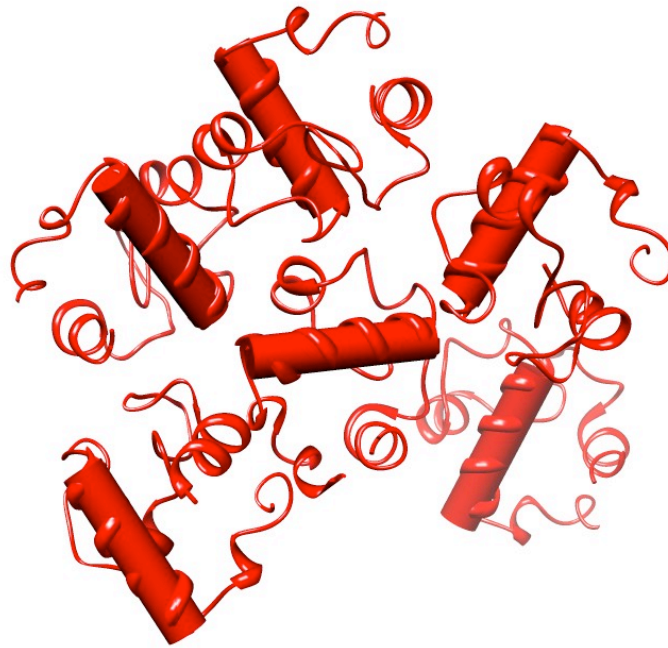


B)



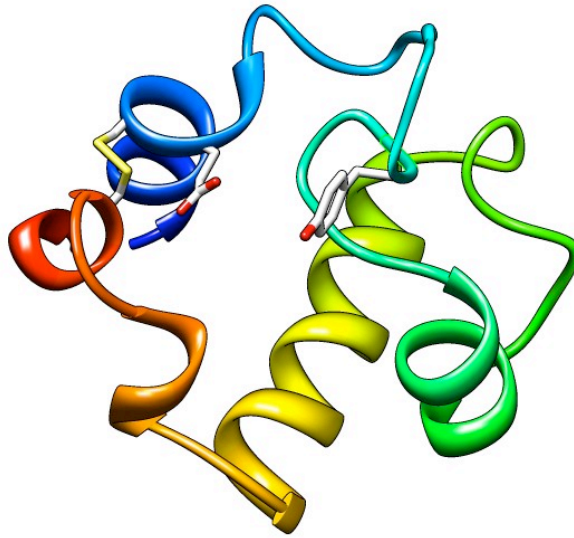
A) Analytical Superdex S75 size exclusion elution profile. The two proteins eluted in two separate peaks. B) Coomassie blue-stained gel with fractions 6-10 shows RipA eluted in the first three fractions and RpfE in the last two. The two proteins do not show any size exclusion shift, rejecting the hypothesis of interaction under these conditions.

Figure 2. Six RpfE molecules in the asymmetric unit.



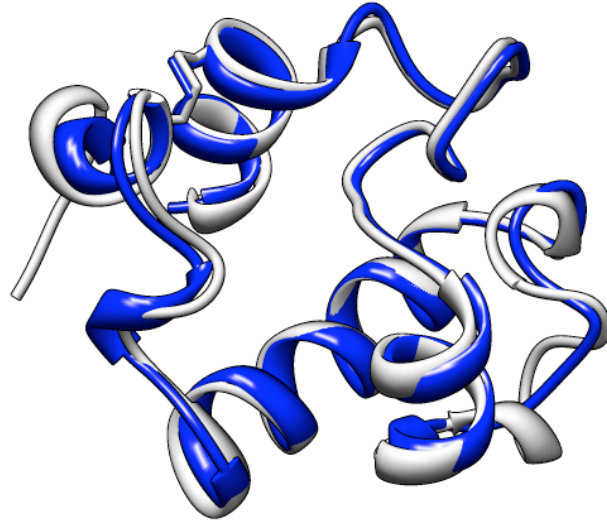
The crystals had the symmetry of space group $P2_12_12_1$ with 6 molecules packed in the asymmetric unit. In this view, the main helix is displayed as a pipe to better elucidate the orientation of each molecule.

Figure 3. Structure of RpfE.



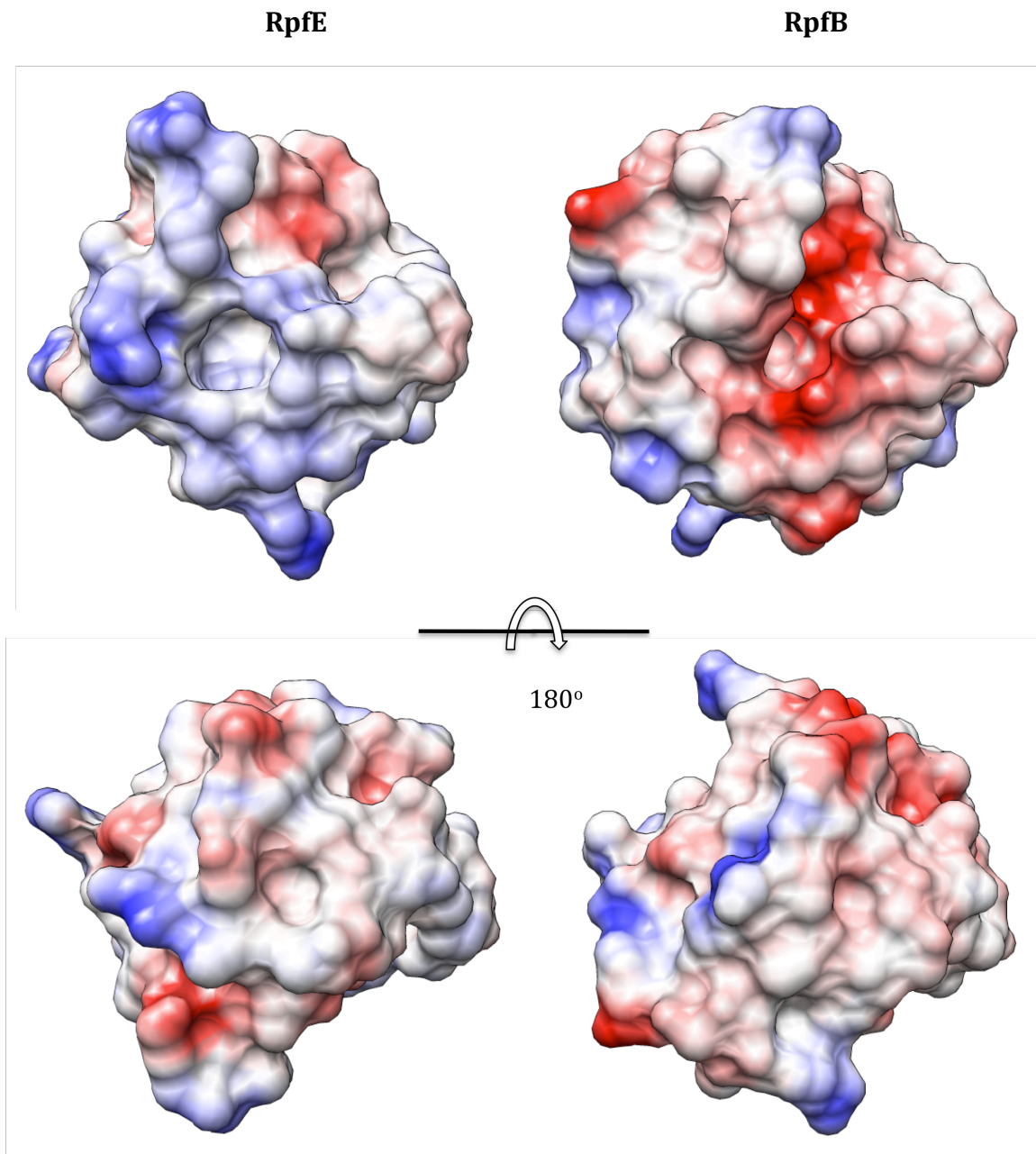
Ribbon diagram of RpfE colored from blue to red from the N-terminus to the C-terminus. The catalytic glutamate and the disulphide bond are highlighted. The RpfE structure is similar to a small lysozyme, but it is classified as a lytic transglycosylase because of the presence of a tyrosine in the catalytic cleft. Instead, in lysozyme, the same position is occupied by an aspartate involved in catalyzing the reaction.

Figure 4. Comparison between RpfE and RpfB.



Superimposition of ribbon representation of RpfB (gray) and RpfE (blue).

Figure 5. Surface comparison between RpfE and RpfB.



RpfE and RpfB present a catalytic cleft with different charge states. The difference in surface potential is also conserved on the surface around the catalytic cleft. Blue and red shading start at + and -5 kT, respectively.

4.8 Tables.

Table 1.

RpFE Data collection	
Space group	P2 ₁
Cell dimensions	<i>a</i> , <i>b</i> , <i>c</i> (Å) 34.54, 84.004, 76.628 α , β , γ (°) 90, 103.528, 90
Resolution (Å)	2.76
Number of molecules in asymmetric unit	6
Refinement	
R-work	0.2374
R-free	0.2882
Ramachandran outliers	0.5% (0.2%)
Ramachandran favored	96.6% (98%)
Rotamer outliers	5% (1%)
C-beta outliers	0
Overall score	2.47

4.9 References.

- ¹ Mukamolova GV, Kaprelyants AS, Young DI, Young M, Kell DB. (1998). A bacterial cytokine. *Proc Natl Acad Sci USA* , 95, 8916-21.
- ² Mukamolova GV, Kormer SS, Kell DB, Kaprelyants AS. (1999). Stimulation of the multiplication of *Micrococcus luteus* by an autocrine growth factor. *Arch Microbiol. , Jul;172(1)*, 9-14.
- ³ Kana BD, Mizrahi V. (2010). Resuscitation-promoting factors as lytic enzymes for bacterial growth and signaling. *FEMS Immunol Med Microbiol. , Feb;58(1)*; 39-50.
- ⁴ Tufariello JM, Jacobs WR Jr, Chan J. (2004). Individual *Mycobacterium tuberculosis* resuscitation-promoting factor homologues are dispensable for growth in vitro and in vivo. *Infect Immun , Jan;72(1)*, 515-26.
- ⁵ Tufariello JM, Mi K, Xu J, Manabe YC, Kesavan AK, Drumm J, Tanaka K, Jacobs WR Jr, Chan J. Source . (2006). Deletion of the *Mycobacterium tuberculosis* resuscitation-promoting factor Rv1009 gene results in delayed reactivation from chronic tuberculosis. *Infect Immun , May;74(5)*, 2985-95.
- ⁶ Downing KJ, Betts JC, Young DI, McAdam RA, Kelly F, Young M, Mizrahi V. (2004). Global expression profiling of strains harbouring null mutations reveals that the five rpf-like genes of *Mycobacterium tuberculosis* show functional redundancy. *Tuberculosis (Edinb) , 84(3-4)*, 167-79.
- ⁷ Beste DJ, Espasa M, Bonde B, Kierzek AM, Stewart GR, McFadden J. (2009). The genetic requirements for fast and slow growth in Mycobacteria. *PLoS One , Apr 28;4(4)*; e5349.
- ⁸ Shah IM, Laaberki MH, Popham DL, Dworkin J. (2008). A eukaryotic-like Ser/Thr kinase signals bacteria to exit dormancy in response to peptidoglycan fragments. *Cell. , Oct 31;135(3)*, 486-96.
- ⁹ Alber T. (2009). Signaling mechanisms of the *Mycobacterium tuberculosis* receptor Ser/Thr protein kinases. *Curr Opin Struct Biol. , Dec;19(6)*, 650-7.
- ¹⁰ Hett EC, Chao MC, Steyn AJ, Fortune SM, Deng LL, Rubin EJ. (2007). A partner for the resuscitation-promoting factors of *Mycobacterium tuberculosis*. *Mol Microbiol. , Nov;66(3)*, 658-68.
- ¹¹ Hett EC, Chao MC, Deng LL, Rubin EJ. (2008). A mycobacterial enzyme essential for cell division synergizes with resuscitation-promoting factor. *PLoS Pathog. , Feb 29;4(2)*, e1000001.
- ¹² Annis I, Hargittai B, Barany G. (1997). Disulfide bond formation in peptides. *Methods Enzymol. , 289*, 198-221.
- ¹³ McPherson A. (2001). A comparison of salts for the crystallization of macromolecules. *Protein Sci. , February; 10(2)*, 418-422.
- ¹⁴ Bolanos-Garcia VM, Chayen NE. (2009). New directions in conventional methods of protein crystallization. *Prog Biophys Mol Biol. , Nov;101(1-3)*, 3-12.
- ¹⁵ Ruggiero A, Tizzano B, Pedone E, Pedone C, Wilmanns M, Berisio R. (2009). Crystal structure of the resuscitation-promoting factor (DeltaDUF)RpfB from *M. tuberculosis*. *J Mol Biol. , Jan 9;385(1)*, 153-62.
- ¹⁶ Brenner S.E. (1998). Practical database searching. *Trends in Biotechnology , 16*, 9-12.

-
- ¹⁷ Cole ST, Brosch R, Parkhill J, Garnier T, Churcher C, Harris D, Gordon SV, Eiglmeier K, Gas S, Barry CE 3rd, Tekaia F, Badcock K, Basham D, Brown D, Chillingworth T, Connor R, Davies R, Devlin K, Feltwell T, Gentles S, Hamlin N, Holroyd S, Hornsby T, Jage. (1998). Deciphering the biology of *Mycobacterium tuberculosis* from the complete genome sequence. *Nature*, 393(6685), 537-44.
- ¹⁸ Russell-Goldman E, Xu J, Wang X, Chan J, Tufariello JM. (2008). A *Mycobacterium tuberculosis* Rpf double-knockout strain exhibits profound defects in reactivation from chronic tuberculosis and innate immunity phenotypes. *Infect Immun.*, Sep;76(9), 4269-81.
- ¹⁹ Hett EC, Rubin EJ. (2008). Bacterial growth and cell division: a mycobacterial perspective. *Microbiol Mol Biol Rev.*, Mar;72(1), 126-56.
- ²⁰ MacDowell, A. A., Celestre, R. S., Howells, M., McKinney, W., Krupnick, J., Cambie, D., Domning, E. E., Duarte, R. M., Kelez, N., Plate, D. W., Cork, C. W., Earnest, T. N., Dickert, J., Meigs, G., Ralston, C., Holton, J. M., Alber, T., Berger, J. M., Agar. (2004). Suite of three protein crystallography beamlines with single superconducting bend magnet as the source. *Journal of synchrotron radiation*, 11, 447-455.
- ²¹ Adams PD, Afonine PV, Bunkóczi G, Chen VB, Davis IW, Echols N, Headd JJ, Hung LW, Kapral GJ, Grosse-Kunstleve RW, McCoy AJ, Moriarty NW, Oeffner R, Read RJ, Richardson DC, Richardson JS, Terwilliger TC, Zwart PH. (2010). PHENIX: a comprehensive Python-based system for macromolecular structure solution. *Acta Crystallogr D Biol Crystallogr.*, Feb;66(Pt 2), 213-21.
- ²² Pettersen, E. F., Goddard, T. D., Huang, C. C., Couch, G. S., Greenblatt, D. M., Meng, E. C., and Ferrin, T. E. (2004). UCSF Chimera--a visualization system for exploratory research and analysis. *J Comput Chem*, 25, 1605- 1612.